HHS Public Access

Author manuscript

Cell Rep. Author manuscript; available in PMC 2024 March 12.

Published in final edited form as:

Cell Rep. 2023 October 31; 42(10): 113189. doi:10.1016/j.celrep.2023.113189.

A bacterial pathogen induces developmental slowing by high reactive oxygen species and mitochondrial dysfunction in *Caenorhabditis elegans*

Zeynep Mirza[1], **Albertha J.M. Walhout**[1,2,3,*], **Victor Ambros**[1,*]

[1]Program in Molecular Medicine, University of Massachusetts Chan Medical School, Worcester, MA 01605, USA

[2]Department of Systems Biology, University of Massachusetts Chan Medical School, Worcester, MA 01605, USA

[3]Lead contact

SUMMARY

Host-pathogen interactions are complex by nature, and the host developmental stage increases this complexity. By utilizing *Caenorhabditis elegans* larvae as the host and the bacterium *Pseudomonas aeruginosa* as the pathogen, we investigated how a developing organism copes with pathogenic stress. By screening 36 *P. aeruginosa* isolates, we found that the CF18 strain causes a severe but reversible developmental delay via induction of reactive oxygen species (ROS) and mitochondrial dysfunction. While the larvae upregulate mitophagy, antimicrobial, and detoxification genes, mitochondrial unfolded protein response (UPR^{mt}) genes are repressed. Either antioxidant or iron supplementation rescues the phenotypes. We examined the virulence factors of CF18 via transposon mutagenesis and RNA sequencing (RNA-seq). We found that non-phenazine toxins that are regulated by quorum sensing (QS) and the GacA/S system are responsible for developmental slowing. This study highlights the importance of ROS levels and mitochondrial health as determinants of developmental rate and how pathogens can attack these important features.

Graphical abstract

*Correspondence: marian.walhout@umassmed.edu (A.J.M.W.), victor.ambros@umassmed.edu (V.A.).

AUTHOR CONTRIBUTIONS

Z.M., A.J.M.W., and V.A. designed the experiments. Z.M. conducted the experiments. A.J.M.W. and V.A. supervised the experiments and wrote the manuscript with Z.M.

DECLARATION OF INTERESTS

The authors declare no competing interests.

SUPPLEMENTAL INFORMATION

Supplemental information can be found online at https://doi.org/10.1016/j.celrep.2023.113189.

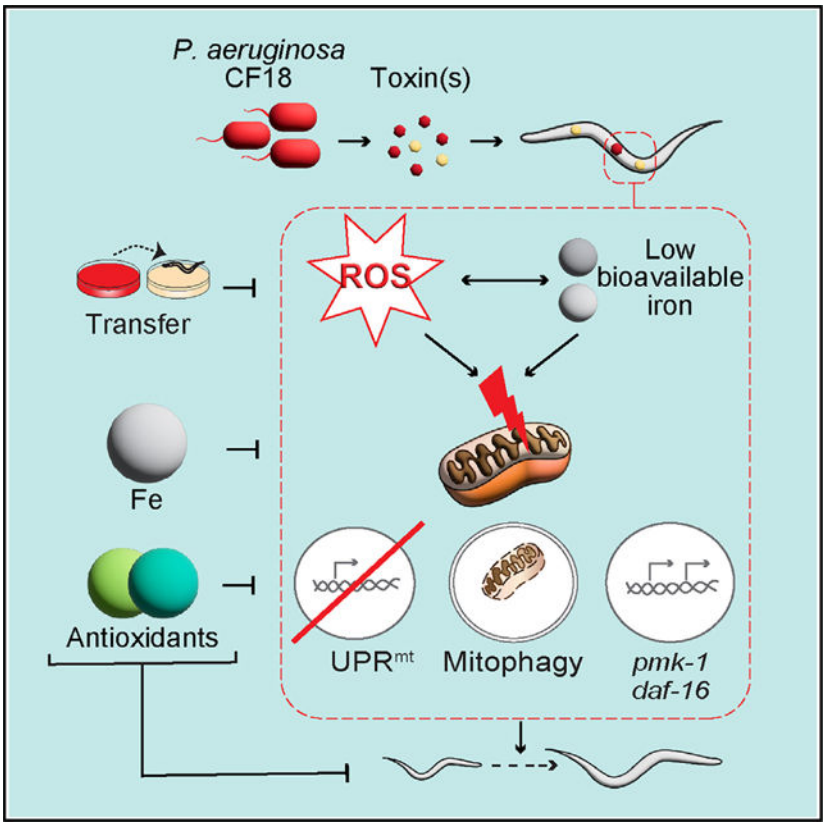

In brief

Mirza et al. show that a *P. aeruginosa* strain reversibly slows development of *C. elegans* via non-phenazine toxins that induce ROS, disturb iron homeostasis, and cause mitochondrial dysfunction. While the UPR^{mt} is repressed, the animals turn on mitophagy, detoxification, and immune defense genes to cope with this pathogenic stress.

INTRODUCTION

Animals and pathogenic bacteria routinely interact in the wild, and these interactions involve conflicting and adaptive responses. Host age is a determinant of the outcome of these interactions because vulnerabilities are more pronounced in developing and older animals, possibly because of immature defense systems and immunosenescence, respectively.[1,2] How a developing organism ensures survival under pathogenic stress while maintaining developmental and reproductive potential is poorly understood.

Caenorhabditis elegans is a valuable model organism to study development and host-pathogen interactions because of its fast development time and genetic tractability and because it is a microbivore. It develops in ~2 days at 25°C: a fertilized egg hatches, and the animal develops through four larval stages (L1–L4) to reach the reproductive adult stage.[3–5] *C. elegans* developmental rate, survival, and other life-history traits can be affected by bacterial diet.[6,7] The animal can distinguish bacteria that support growth and learn to avoid bacteria with poor nutritional value.[8] *C. elegans* is susceptible to many

pathogens, including the opportunistic human pathogen *Pseudomonas aeruginosa*, and the animal possesses conserved innate immunity pathways, such as the p38 mitogen-activated protein kinase (MAPK) pathway.[9] When *C. elegans* adapts to nutritional and pathogenic factors, there can be trade-offs, including reduced fecundity and accelerated development as well as immune system activation and somatic lipid loss.[6,10,11]

Pathogens target various cellular processes and organelles in the host, including iron-rich mitochondria.[12] Mitochondria are the powerhouses of cells and a major source of reactive oxygen species (ROS). At physiological levels, ROS serve as signaling molecules; however, at higher levels, ROS are detrimental, causing the oxidation of biomolecules and the disruption of iron homeostasis.[13] Most organisms maintain iron levels within a narrow range. Low iron interferes with core functions, including energy production and DNA synthesis; high iron increases ROS via the Fenton reaction.[14–16] A recent study showed that 244 *Escherichia coli* mutants that have low bioavailable iron, either because of high ROS or defects in iron uptake/utilization, cause oxidative stress and mildly slow *C. elegans* larval development. Antioxidants or iron supplementation rescue this slow larval development.[17] These results indicate that optimum growth requires maintaining the balance between ROS and iron levels.

Upon detection of mitochondrial dysfunction, hosts transcriptionally activate the mitochondrial unfolded protein response (UPR^{mt}), which results in the induction of genes involved in ROS detoxification, recovery of oxidative phosphorylation, and chaperones that re-establish mitochondrial proteostasis.[18,19] *C. elegans* also activates anti-microbial and xenobiotic detoxifying pathways.[20]

P. aeruginosa has numerous virulence regulators, including three QS systems, Las, Rhl, and Pqs,[21] and a GacA/S two-component system,[22] which allow the pathogen to utilize a wide range of virulence factors under different conditions. These virulence factors include toxins that damage mitochondria or induce ROS, including phenazines and hydrogen cyanide (HCN).[23,24] Phenazines are redox-active, diffusible, small compounds that cause ROS production and oxidative stress in recipient cells.[25] HCN exerts its toxicity through the inhibition of the electron transport chain.[26]

Here, we asked whether any of 36 *P. aeruginosa* strains affect *C. elegans* larval developmental rates. We focused on the CF18 strain, which dramatically but reversibly slows the animal's development by high ROS levels and mitochondrial dysfunction. Remarkably, however, the UPR^{mt} was not activated; instead, mitophagy genes were induced. We found that CF18 utilizes non-phenazine toxin(s) that are under the control of both QS and the GacA/S system.

RESULTS

Three groups of *P. aeruginosa* strains that affect *C. elegans* developmental rate

Different *P. aeruginosa* strains have different degrees of virulence toward adult *C. elegans*; however, their effects on larval development have not been examined.[27] We fed L1 larvae 36 *P aeruginosa* strains and observed three main *C. elegans* larval developmental effects:

normal, moderately slow, and slow development, which were defined as larvae reaching adulthood in 2 (25), 3 (8), or more than 3 days (3), respectively (Figures 1A and 1B; Table S1). The CF18 strain caused the most severe developmental delay; none of the larvae reached adulthood after more than 85 h. Strains with strong virulence for adult worms also delay larval development; however, strains with moderate adult virulence can be tolerated by larvae (Figure 1C), indicating that adult and larval phenotypes can be uncoupled, which likely reflects partly distinct mechanisms.

We investigated whether there is a correlation between the degree of larval development slowing and the bacterial growth rate. We reasoned that fast-growing bacteria could reach a high bacterial density, leading to the production of QS-related virulence factors earlier than slower-growing strains, or that slow-growing bacteria could form thinner lawns, which may cause reduced bacterial intake. We found that the degree of developmental slowing in *C. elegans* did not correlate with the bacterial growth rate (Figure S1A).

P. aeruginosa CF18 causes reversible developmental slowing

None of the *C. elegans* larvae fed CF18 reached adulthood at day 3. Visual inspection showed that most of the animals appeared to be stalled at the L2 stage. The *Plag-2::GFP* reporter is expressed in the distal tip cells,[28,29] and we observed a slow but steady increase in gonad length relative to body length over time when we fed this strain with CF18, showing that development is not arrested but, rather, extremely slow (Figures 1D and S1B). *hlh-8::GFP* is expressed in M cells,[30] a single blast cell that gives rise to all postembryonic mesodermal cells.[3] We found that M cell divisions are already delayed in CF18-fed larvae at the 6-h time point (Figure 1E), indicating that developmental slowing begins shortly after CF18 exposure.

Under stressful conditions, *C. elegans* can develop into a stress-resistant and long-lived alternative third larval stage called dauer diapause.[31] We evaluated whether CF18-fed larvae form dauers that are resistant to SDS treatment. Our results showed that CF18-fed animals did not form dauers (Figure S1C).

Larvae fed CF18 for up to 3 days resumed normal development when transferred to non-pathogenic bacteria (Figures 1F and S1D). These animals developed into fully reproductive adults whose survival was similar to animals raised on non-pathogenic bacteria (Figures S1E and S1F). Thus, larvae maintain full developmental potential while exposed to CF18, and adults exhibit no apparent fitness cost from CF18-induced developmental slowing early in life.

Developmental delay is a result of CF18 pathogenicity

To assess the mechanism of developmental slowing by CF18, we first examined whether slowing could be attributed to a deficiency of this bacterial strain in nutrient(s). We reasoned that ultraviolet (UV) treatment of CF18 would inactivate UV-labile compounds but should not alleviate any nutritional deficiencies CF18 may have. UV irradiation (0.15 J) reduced the number of bacterial colony-forming units (CFUs) from 6.45E+10 CFUs/plate to 1.79E+05 CFUs/plate, showing that UV radiation has a potent effect on bacteria (Figure S1G). Strikingly, larvae developed faster on UV-treated CF18 lawns compared with

unirradiated lawns, indicating that slowing requires the activity of live CF18 bacteria and further suggesting that developmental slowing caused by CF18 could not be attributed to a deficiency of this bacterial strain in nutrient(s) essential for normal *C. elegans* development (Figure 1G). UV treatment of CF18 would be expected to inactivate UV-labile compounds but should not alleviate nutritional deficiencies.

Many *P. aeruginosa* strains secrete pathogenic compounds, including phenazines, siderophores, rhamnolipids, and proteases.[22] In our assays, bacterial plates were pre-incubated for 2 days before adding larvae, which enabled an accumulation of secreted compounds. To determine whether bacterially secreted compounds play a role in developmental slowing, we transferred the bacterial lawn grown for 2 days to fresh plates, immediately added larvae, and compared their growth rates with those that had been cultured on undisturbed CF18 plates. We found that larvae grown on bacteria that had been transferred developed faster than control larvae (Figure 1G). These results indicate that developmental slowing by CF18 requires one or more secreted compounds. To rule out other potentially contributing factors, such as biofilm disruption and reduced bacterial CFUs during transfer, we collected and re-plated the lawn to original plates. Bacteria re-plated to the original plates slowed development in a manner comparable with undisturbed plates (Figure S1H). We also confirmed that the number of bacteria transferred was comparable with the undisrupted plates (Figure S1G).

P. aeruginosa gacA mutants display attenuated virulence in mouse, *Arabidopsis*, and adult *C. elegans* infection models.[32,33] To verify that developmental slowing is a result of virulence, we created a CF18 *gacA* mutant and found that animals fed this strain exhibited a normal development rate (Figures 1I and 1J). This result confirms that slow development is a result of active bacterial pathogenesis.

P. aeruginosa PA14 colonizes the gut in L4 and adult animals but not earlier larval stages.[32] Therefore, we examined whether the larval gut was colonized by CF18 in developmentally slowed L1 and L2 larvae. CF18-fed larvae exhibited no gut colonization by bacteria (average of 0–20 bacteria/larva) for up to 96 h. Animals fed PA14 or HB101 exhibited a similar number of live bacteria in their gut as CF18-fed larvae in early larval stages. The guts of the PA14 and HB101-fed animals became colonized over time as they progressed to the L4 and adult stages. Because CF18-fed larvae did not develop beyond the L3 stage, their gut remained uncolonized (Figure 1H).

Transcriptome analysis of CF18-fed larvae shows upregulation of genes involved in immune defense and mitophagy

We hypothesized that CF18-fed larvae may activate the expression of pathogen-defense genes and other programs that enable them to cope with virulence factors and maintain their developmental potential. We compared the transcriptomes of larvae fed wild-type (WT) CF18 and CF18 *gacA* mutant bacteria after 4 and 6 hours of feeding.

A total of 2,428 genes were differentially expressed between 4-h WT CF18 and 4-h CF18 *gacA*-fed larvae: 1,240 genes were upregulated, and 1,188 genes were downregulated. Usingthe database for annotation, visualization and integrated discovery (DAVID)[34] and

WormCat,[35] we found that autophagy-, mitophagy-, detoxification-, and immune defense-related genes are elevated in larvae fed WT CF18 compared with larvae fed CF18 *gacA* as early as after 4 h of exposure (Figures 2A and S2A). In addition, genes related to cell division, DNA replication, and translation were reduced in animals fed WT CF18, consistent with their slowed development (Figure S2B). We obtained similar results by comparing differentially expressed genes between 6-h WT CF18-fed and 6-h CF18 *gacA*-fed larvae (Figures S2C and S2D).

We found a significant overlap among the genes reported to be differentially expressed in adult animals fed PA14[36] and larvae fed CF18 for 4 h (Table S2). Moreover, genes that were differentially expressed in WT CF18-fed larvae significantly overlapped with *pmk-1* and *daf-16*-dependent genes identified in other studies.[36,37] Thus, both larvae and adult animals turn on their *daf-16*-dependent detoxification and *pmk-1*-dependent immune system gene expression upon exposure to *P. aeruginosa*.

CF18 causes mitochondrial dysfunction and high ROS in *C. elegans* larvae

The observation that mitophagy genes are upregulated in CF18-fed larvae suggests that these animals experience mitochondrial dysfunction. To distinguish whether the induction of mitophagy is a protective response or a part of CF18 pathogenesis, we examined the recovery and survival of *C. elegans* mitophagy mutants (*pink-1(ok3538)*, *dct-1(luc194)*, and *pdr-1(gk448)*) on CF18. Mitophagy mutants exhibited shorter survival compared with WT animals when fed with CF18 (Figure 2B). Additionally, after 2 days of CF18 exposure, mitophagy mutant larvae transferred to non-pathogenic bacteria exhibited significantly reduced rates of recovery compared with the WT animals (Figure 2C). Thus, mitophagy is beneficial to larvae and required for survival on CF18 and for recovery after transfer to non-pathogenic bacteria.

To examine the mitochondrial health of CF18-fed larvae, we first measured oxygen consumption rates (OCRs) of larvae fed various bacteria. While we did not observe a difference in OCR values for larvae fed for 1 h, a difference in OCR values emerged by 2 h of feeding (Figures S3A and S3B). Basal and maximal OCR values were significantly lower in CF18-fed larvae than CF18 *gacA*-fed larvae after 4 h of feeding. While larvae fed PA14 (a moderately slowing strain) also exhibited low basal and maximal OCR values, there was a small but statistically significant difference between basal OCR rates for CF18- vs. PA14-fed larvae. (Figures 2D and 2E).

To investigate the mitochondrial membrane potential ($\Delta\Psi m$) of CF18-fed larvae, we used tetramethylrhodamine ethyl ester perchlorate (TMRE), which is a positively charged dye that accumulates in healthy mitochondria because of its negative charge.[38,39] Depolarized mitochondria fail to accumulate this dye.[39] $\Delta\Psi m$ is generated by electron transport chain (ETC) complexes I, III, and IV by pumping H^+ ions across the inner membrane to the intermembrane space and is then utilized by complex V to generate ATP.[40] In addition to generating ATP, $\Delta\Psi m$ is required for mitochondrial transport.[40] $\Delta\Psi m$ is maintained in a stable range, and disturbances in $\Delta\Psi m$ indicate mitochondrial dysfunction. TMRE staining showed that the mitochondria of CF18-fed larvae depolarized in comparison with CF18 *gacA*-fed larvae, which readily accumulate TMRE (Figure 2F).

Mitochondria are dynamic organelles: they regularly undergo fusion and fission, and mitochondrial morphology is an indicator of their health.[38] We assessed the morphology of the mitochondrial network of body wall muscle as described by Sarasija and Norman.[38] The mitochondrial network was fragmented in CF18-fed larvae, while *gacA*-fed larvae had a healthy linear mitochondrial network (Figure 2G). These results confirm that CF18 induces mitochondrial dysfunction.

Because mitochondria are the main source of ROS, and because defective mitochondria can produce higher levels of ROS,[41,42] we measured ROS levels of larvae fed CF18, PA14, or CF18 *gacA* mutants using MitoSOX Red.[42] We found that the level of ROS was higher in CF18-fed larvae than CF18 *gacA*-fed larvae, and larvae fed PA14 had intermediate levels of ROS (Figure 2H). Using a second ROS-detecting dye, 6-carboxy-2′,7′-dichlorodihydrofluorescein diacetate (H2-DCFDA), we confirmed that CF18-fed larvae had elevated levels of ROS (Figure S3C). These results show a correlation between developmental slowing and ROS levels in larvae.

To examine whether high ROS levels accompany other types of developmental slowing, we conducted a small survey of 21 RNAi clones that target a diverse class of genes and slow development.[43,44] We found that 9 of 21 RNAi clones, belonging to “protein synthesis, transcription factor, metabolism, mitochondrial function” classes,[43,44] induced high ROS, and 12 of 21 slowed larval development without elevated ROS levels (Figure S3D). Thus, high ROS levels do not necessarily accompany all modes of developmental slowing.

UPR^{mt} is not induced in larvae fed CF18

To test whether mitochondrial dysfunction and mitophagy in CF18-fed larvae are accompanied by induction of the protective UPR^{mt}, we examined the expression of UPR^{mt} reporters. Surprisingly, two signature UPR^{mt} genes, *hsp-6* and *hsp-60*,[45] were not induced in CF18-fed larvae (Figures 2I and 2J). The mitochondrial superoxide dismutase SOD-3, which neutralizes superoxide in the mitochondria and is regulated by the *daf-2* insulin-like signaling pathway,[46] was also not induced in CF18-fed larvae (Figure 2K). Thus, mitochondrial dysfunction is not coupled to conventional mitochondrial damage response in CF18-fed animals.

We next asked whether activation of UPR^{mt} by mutation may restore mitochondrial function, reduce ROS production, and consequently allow larvae to develop faster. We tested *atfs-1(et15)* and *zip-3(gk3164) C. elegans* mutants that have constitutively active UPR^{mt}[47] and found that both mutant animals did not develop faster than WT animals, showing that activation of UPR^{mt} is not sufficient to overcome CF18-induced developmental slowing (Figure 2L).

Antioxidants and iron supplementation prevent CF18-induced *C. elegans* mitochondrial dysfunction and developmental slowing

To further test whether increased ROS levels contribute to developmental delay, we supplemented plates with either of two antioxidants, N-acetyl cysteine (NAC) or resveratrol, which alleviate high ROS in *C. elegans*.[17,48] Both antioxidants rescued developmental slowing in a dose- and time-dependent manner (Figures 3A and 3B), while they had

no effect on the developmental phenotype of the *gacA*-fed larvae (Figures 3C and 3D). Antioxidants also restored the ΔΨm of CF18-fed larvae (Figure 3E).

Next, we assessed the role of iron because iron influences mitochondrial health and ROS generation and is also required for *C. elegans* development.[15,17,49] We found that supplementing the medium of CF18-fed animals with ferric chloride partially rescued developmental slowing, although less efficiently than antioxidants (Figures 3F and 3G). Iron supplementation also improved ΔΨm of larvae fed CF18 in a dose-dependent manner (Figure 3E). NAC and ferric chloride did not inhibit bacterial growth at the doses used (Figures S3E and S3F).

While we did not observe a correlation between bacterial ROS levels and larval developmental rates (Figure 3H), we did find that developmental phenotypes are correlated with larval ROS levels (Figure 2H). NAC and, to a lesser extent, iron supplementation significantly reduced ROS levels of CF18-fed larvae (Figure 3I). These results show that ROS levels are elevated in CF18-fed larvae and that supplementing antioxidants or iron reduces these levels.

To test whether pharmacological induction of high ROS and/or low iron in animals fed non-pathogenic bacteria could phenocopy the developmental slowing by CF18, we used paraquat to induce mitochondrial ROS[50,51] and the iron-specific chelator bipyridine (BP) to disrupt iron homeostasis. We observed dose-dependent developmental slowing under both conditions (Figures 4A and 4B). Both paraquat and BP increased ROS and reduced TMRE accumulation in mitochondria relative to their respective controls (Figures 4C and 4D). Importantly, similar to larvae fed CF18, animals exposed to paraquat or BP can resume development when transferred to plates lacking these chemicals (Figures 4E and 4F). Taken together, these results show that imbalances in iron homeostasis and high levels of ROS induce reversible developmental slowing in *C. elegans*.

Because iron metabolism and ROS levels are interconnected—high ROS cause low iron bioavailability[17] and low iron levels cause high ROS[52]—we assessed whether either the iron imbalance or the high ROS levels alone could account for developmental slowing. We tested whether iron supplementation could rescue paraquat-induced developmental slowing and whether NAC could rescue BP-induced developmental slowing. Iron supplementation showed minimal rescue of developmental slowing at one-third of the paraquat dose (25 mM) that we used in our experiments (Figure 4G), while it was ineffective for the full paraquat dose (75 mM) (Figure S3G). Similarly, NAC supplementation was ineffective for the full BP dose (150 μM) (Figure S3H), and it partially alleviated the developmental slowing induced by half the dose of BP (75 μM) (Figure 4H). These results imply that, while there is an interaction between iron metabolism and ROS levels, iron imbalance and high ROS levels individually contribute to developmental slowing rather than converging on a single mechanism.

Last, we used the intracellular Mg^{2+} indicator Magnesium Green AM and the mitochondrion-specific Ca^{2+} indicator dye Rhodamine 2 AM to investigate whether Mg^{2+} and Ca^{2+} balance is changed in CF18- and CF18 *gacA*-fed larvae because these divalent

cations affect bioenergetics and mitochondrial ROS production.[53–55] We did not find a difference in Magnesium Green fluorescence levels in CF18- and CF18 *gacA*-fed larvae (Figures S3I and S3J). Rhodamine 2 AM did not show mitochondrial localization, and there was no difference in total Rhodamine 2 AM fluorescence in the intestine of CF18- and CF18 *gacA*-fed larvae. Consequently, we cannot conclude whether the calcium balance was changed in CF18-fed larvae (Figures S3K and S3L).

Phenazines are not involved in CF18-mediated developmental slowing

Next, we asked which bacterial factors cause high ROS and mitochondrial dysfunction in CF18-fed larvae. We first considered phenazines, secondary metabolites of *Pseudomonas* that can induce high ROS and mitochondrial dysfunction in recipient cells.[56,57] CF18, like many other *P. aeruginosa* strains, contains two redundant phenazine biosynthesis operons, *phzA1-G1* (*phz1*) and *phzA2-G2* (*phz2*), which are regulated by three QS (*Las*, *Rhl*, and *PqS*) and the *GacA/S* two-component system.[58,59] We deleted the two phenazine operons and fed this double mutant to *C. elegans* larvae. Surprisingly, larvae still developed slowly on this mutant, antioxidant and iron supplementation still rescued this phenotype, and $\Delta\Psi m$ was still disrupted (Figures 5A and 5B). In CF18 *Δphz1–2*-and WT CF18-fed larvae, ROS levels were similar. PA14 *Δphz1–2*-fed larvae showed a slight reduction in ROS compared with WT PA14-fed larvae but still exhibited higher ROS levels than fully attenuated CF18 *gacA*-fed larvae. (Figure 5C). These results show that phenazines are not critical components of CF18-induced developmental slowing.

Biofilm, chemotaxis, and type VI secretion systems are upregulated in WT CF18 compared with the CF18 *gacA* mutant

Because the *GacA/S* system is required for full virulence, we asked whether other bacterial genes regulated by this system are important for developmental slowing in *C. elegans*. We compared bacterial gene expression in WT CF18 relative to CF18 *gacA* mutants and identified 252 upregulated and 166 downregulated genes in WT CF18. Enrichment analysis showed that type VI secretion-related and chemotaxis genes are increased in expression in WT CF18 bacteria (Figure 5D), whereas siderophore biosynthesis genes are decreased (Figures 5D, S4A, and S4B). Siderophores are iron-scavenging molecules, and *P. aeruginosa* produces two types: pyoverdine and pyochelin.[60] These results suggest that CF18 may not be experiencing iron starvation. Because the CF18 genome is poorly annotated, we also manually inspected the upregulated genes in WT CF18, focusing on potential mitochondrial toxins and toxin delivery systems. This led us to focus on type VI (subtype H1 and H3) toxin delivery systems, which showed about 5-fold enrichment in gene enrichment analysis, and HCN biosynthesis genes, which increased about 2-fold in WT CF18 (Figures 5E–5G).

The type VI secretion system is a versatile toxin delivery system that can target both prokaryotic and eukaryotic cells.[61] *P. aeruginosa* possesses three type VI secretion systems: H1-T6SS, H2-T6SS, and H3-T6SS.[61,62] While the H1 and H3-T6SS genes are among the genes upregulated most in WT CF18 compared with *gacA*, H2-T6SS was not differentially expressed. We created H1 and H3-T6SS mutants by deleting parts of the operon encoding the core structural components and found that larvae fed these mutants were still developmentally delayed, and iron or antioxidant supplementation still rescued

this phenotype (Figure 5H). Therefore, these toxin delivery systems are not involved in mediating developmental slowing by CF18.

Based on the 2-fold upregulation in our bacterial RNA sequencing (RNA-seq) data and a literature search of known mitochondrial toxins of *P. aeruginos*a, HCN was a second toxin candidate. HCN inhibits mitochondrial respiration and causes high ROS levels.[63–65] We created a CF18 deletion mutant of the HCN synthase operon but again observed neither alleviation in developmental slowing of *C. elegans* larvae nor an increase in OCR rate; moreover, supplementation of either iron or NAC still rescued this phenotype (Figures 5H and 5I).

CF18 genes required for developmental delay of *C. elegans*

To identify bacterial genes that are required for the slowing of *C. elegans* larval development, we created a mariner C9 transposon insertion library[66] of ~10,000 CF18 mutants.[66] We screened this library in triplicate using transgenic animals carrying *Pcol-19*:*GFP*, which is expressed at the L4 molt,[67] thus allowing us to visually identify animals that have completed larval development (Figure 6A). We obtained 66 independent mutants that each carry a single transposon insertion in one of 42 different genes, which are hereafter referred to as “hits.” We manually grouped these hits into eight categories: QS, two-component system, motility, purine metabolism, pyrimidine metabolism, amino acid metabolism, propionate metabolism, and other (Figure 6B).

We found hits in all three QS systems—specifically *lasI*, *lasR*, *rhlR*, *pqsR*, and *pqsB*—all of which support normal *C. elegans* development. Both *gacA* and *gacS* mutants were found and, as expected, fully rescued development.[69] We identified four genes involved in amino acid metabolism: *liuA*, *liuB*, *liuE*, and *liuR*, which are required for leucine breakdown; *trpC* and *trpF*, which are required for tryptophan metabolism; and *cysQ*, which is involved in cysteine metabolism. We also found two genes that are required for propionic acid breakdown: *prpB* and *prpC*. This result suggests that amino acid breakdown products may be involved in synthesizing the CF18 toxin(s).

Another group of hits belongs to purine biosynthesis pathways; we obtained multiple alleles of the *de novo* purine biosynthesis genes *purH*, *purL*, *purM*, and *purK*. While these purine mutants formed thinner lawns, they were fully permissive to normal development. We supplemented these mutants with each of four nucleobases—adenine, guanine, thymine, and cytidine—and found that only adenine supplementation restored the pathogenicity of the CF18 purine mutants (Figures 6C–6E). Nucleobase supplementation had no effect on non-purine mutants or WT CF18 (Figures 6F, S5A, and S5B). Importantly, we found that using a higher bacterial density of slow-growing mutants did not restore the pathogenicity of these mutants (Figure 6G). Overall, pathogenicity restoration of the purine mutants by metabolite supplementation, rather than increasing cell density, suggests that core metabolic processes are relevant and necessary for full virulence of CF18.

Our mutants showed varying degrees of attenuation of developmental slowing compared with the WT CF18 (Figure 6H and S5C). We found that most of the mutants attenuated for

larval slowing showed varying degrees of attenuation for adult survival, suggesting that most of the hits are relevant to both phenotypes (Figure S5D).

P. aeruginosa genes can be grouped into a core genome, present in most strains, and an accessory genome that is less prevalent and differs among strains.[27,70] We wondered whether the higher virulence of CF18 compared with the other strains can be explained by unique accessory genes in CF18. We classified genes that are present in more than 90% of strains as a core genome and genes that were present in fewer than 90% of strains as accessory genes.[27] Only two hits from our screen are part of the accessory genome of CF18, including Q002_01995, which encodes a hypothetical protein, and *pilV*. These genes are present in 50% and 72%, respectively, of the 36 strains tested (Figure 6I). Therefore, we did not identify a virulence gene unique to CF18. Next, we aligned the amino acid sequences of each protein encoded by a hit across the 36 *Pseudomonas* strains tested but did not find any alleles that are unique to CF18 (Data S1).

We compared our CF18 mutants with PA14 adult virulence mutants:[68] Only eight hits were not found in the PA14 screen, most of which are relatively understudied (Figure 6J; Table S3). The large overlap between CF18 and PA14 transposon mutagenesis hits highlights the prevalence of common virulence factors for adult killing by PA14 and larval slowing by CF18.

ROS levels and OCRs correlate with developmental timing in larvae fed partially or fully attenuated CF18 mutants

Larvae fed fully attenuated (causing normal larval growth rate) *rhlR* or *gacA* mutant CF18 exhibited significantly improved OCRs in comparison with WT CF18. Larvae fed partially attenuated CF18 mutants (*ccmB*, *cysQ*, and *fleN*) showed only a slight increase in OCR (Figure 6K). Developmental rates showed a moderate correlation with both basal and maximal OCR (Figures S5E and S5F).

Larvae fed the fully attenuated CF18 *gacA* mutant had low levels of ROS, while larvae fed the partially attenuated CF18 *ccmB* and CF18 *cysQ* mutants had intermediate levels of ROS (Figure 6L), showing that the degree of developmental rate rescue for larvae fed these mutants correlates with larval ROS levels. We confirmed that the bacterial ROS levels of these mutants do not correlate with larval development rates (Figure S5G). These results, along with previous ROS level analyses, show that there is a correlation between larval ROS levels and developmental slowing (Figures 2F, 3I, and 6L).

Antioxidant or iron supplementation does not restore the lifespan of adult animals fed CF18

To compare mechanisms of larval developmental slowing and adult killing, we supplemented plates with doses of NAC or iron and tested the adult lifespan. The adult lifespan on CF18 was not extended by antioxidant or iron supplementation (Figure S6A). In addition, TMRE staining showed that CF18-fed adult animals have disrupted $\Delta\Psi m$ compared with *gacA*-fed animals. While iron supplementation showed no effect on TMRE staining, NAC supplementation slightly improved TMRE accumulation. However, even with NAC supplementation, TMRE staining did not reach the levels of *gacA*-fed animals (Figures

S6B and S6C). Moreover, CF18-fed adult animals have higher amounts of ROS than *gacA*-fed animals (Figures S6D and S6E).

We also observed a small but statistically significant reduction in TMRE staining in CF18-fed adults relative to PA14-fed animals. Moreover, the deletion of phenazine biosynthetic operons in CF18 and PA14 did not change TMRE staining, suggesting that mitochondrial dysfunction in adult animals was also phenazine independent (Figure S6F and S6G). These results indicated that adult animals also experienced increased ROS and mitochondrial dysfunction on CF18; however, iron and NAC supplementation did not restore the $\Delta\Psi m$ to *gacA* levels in adults and failed to extend the lifespan. Thus, high ROS levels and mitochondrial dysfunction affect adults and larvae differently, suggesting somewhat distinct CF18 pathogenicity mechanisms in adults versus larvae.

DISCUSSION

We describe an extreme developmental slowing of *C. elegans* larvae by *P. aeruginosa* CF18, caused by high levels of ROS and rapid loss of mitochondrial function. High levels of ROS can damage a variety of biomolecules, including proteins, nucleic acids, and lipids. In addition, high ROS can result in iron deficiency through the Fenton reaction. Because both antioxidants and iron offered protection against CF18 toxicity, it is likely that iron imbalance contributes to developmental slowing. Consistent with this idea, we find that a strong oxidizing agent or iron chelator confers similar phenotypes as CF18. Importantly, our observation that genes involved in biosynthesis of the iron siderophores pyoverdine and pyochelin were not upregulated in CF18 suggests that iron deficiency occurs predominantly in the larvae and not in the bacteria itself. We were unable to directly measure iron levels in either bacteria or in *C. elegans*;[17] further studies utilizing inductively coupled plasma-mass spectrometry may provide insights into the interplay between oxidizing agents and iron in both CF18 and *C. elegans*.

Surprisingly, CF18-induced mitochondrial dysfunction in *C. elegans* larvae was not accompanied by activation of the protective UPR^{mt}, indicating that mitochondrial dysfunction does not necessarily elicit a universal mitochondrial damage response. The ability of *P. aeruginosa* to suppress the UPR^{mt} reporter *hsp-6p::GFP* in spite of the presence of a mitochondrial insult has been documented previously.[71,72] Instead of activating UPR^{mt}, mitophagy/autophagy pathways were activated in CF18-fed animals, possibly to remove damaged mitochondria and limit ROS production.

It is striking that the developmental delay exhibited by larvae fed CF18 is fully reversible, in that larvae growing on CF18 lawns for up to 3 days rapidly develop into adults when transferred to *E. coli*. The rescued adults exhibit no apparent loss in fecundity or longevity. Moreover, the similar developmental slowing caused by paraquat or BP treatment of larvae growing on *E. coli* food is also reversible. These findings lead us to interpret the developmental slowing as an active adaptive response by the animal to limited energy availability. Development is energetically costly, as are pathogen defense and cellular damage control programs. If mitochondrial dysfunction and elevated ROS levels result in limited energy production, then developmental delay until these conditions are alleviated

would favor survival. In a screen for hypothetical regulators of developmental slowing, we screened ~169,000 haploid genomes but did not recover any viable and reproductive mutants that could bypass developmental slowing on CF18 (Table S4), suggesting that developmental delay is not orchestrated by a single signaling pathway or transcription factor. It is also possible that bypass of developmental delay on CF18 could be larval lethal. Future screens for mutant animals that exhibit loss of fitness or developmental robustness after developmental delay could identify pathways underlying the remarkable ability of larvae to maintain full developmental potential and reproductive fitness during severe metabolic stress.

Previously, several *E. coli* mutants that slowed *C. elegans* larval development have been identified, and this delay could also be rescued by supplementation of antioxidants or iron.[17] However, several observations indicate that the mechanisms involved are distinct between the growth delay caused by these *E. coli* mutants and that caused by CF18. These differences include the following. (1) WT *E. coli* is not toxic to *C. elegans* and therefore does not produce the same toxins as CF18. CF18-induced developmental slowing is a pathogenic process, orchestrated by QS and gacA/S virulence regulators, while developmental delay induced by *E. coli* mutants is a result of dietary iron deficiency. (2) The developmental delay caused by the *E. coli* mutants is relatively mild, while the delay elicited by CF18 is extreme. (3) UPR^{mt} was induced in larvae fed the *E. coli* mutants, whereas UPR^{mt} is repressed and mitophagy is activated in CF18-fed larvae. (4) While the *E. coli* mutants that cause developmental delay have high levels of bacterial ROS, we did not find elevated bacterial ROS in CF18. Instead, our results showed that larvae fed CF18 had high levels of ROS. (5) For CF18-fed larvae, antioxidants alleviate developmental slowing more effectively than iron supplementation does, while iron performs better than antioxidants for *E. coli* fed-larvae. (6) For the *E. coli* mutants, the primary mechanism of larval developmental delay is low bacterial iron; high bacterial ROS is an indirect cause that results in low bacterial iron. For CF18-induced slowing, high larval ROS levels and iron imbalance contribute to developmental slowing, both jointly and independently. (7) Although we could not measure iron levels directly, our results suggest that iron supplementation is most likely to act via the larvae rather than via the bacteria. Siderophore biosynthesis genes are down-regulated in WT CF18 compared with the *gacA* mutant, suggesting that WT CF18 does not experience iron starvation on our assay plates. Additionally, iron-supplemented CF18 remains capable of killing adult animals, suggesting that iron supplementation does not cause attenuation of CF18 (Figure 7). These considerations highlight the partially overlapping and distinct features of the different mechanisms elicited by different bacterial species and strains that lead to changes in *C. elegans* developmental progression.

We investigated potential CF18 virulence factors responsible for larval developmental slowing, employing three methods: a candidate-based approach guided by published literature, bacterial transcriptome analysis, and an unbiased genetic screen using transposon mutagenesis. We created mutants of high-profile suspects based on RNA-seq and literature and ruled out any requirement for phenazines, HCN, or T6SS in developmental slowing. Among our transposon mutagenesis hits that attenuated slowing, we found many virulence regulators, the GacA/S system, and a few understudied transcription factors. In addition, we identified genes whose connection to CF18 virulence is not immediately apparent. We found

that core metabolic processes, such as amino acid metabolism and nucleotide metabolism, are required for full virulence. As exemplified by purine mutants, metabolite deficiency, not low bacterial growth rate, causes attenuation of these mutants. These results suggest that amino acids and/or purines may be used as building blocks for the synthesis of CF18 toxins.

We did not identify any accessory genome determinant for CF18 virulence whose exclusive presence in the CF18 genome can explain the dramatic difference in larval virulence between CF18 and other *P. aeruginosa* strains. It is possible that differences in gene expression, rather than gene content, may underlie the virulence differences between the strains. Future studies comparing the transcriptome of different *P. aeruginosa* strains can address these possibilities. Taken together, our results indicate that the CF18 strain possesses multifactorial and possibly redundant virulence mechanisms that attack a host's energy resources and cause *C. elegans* larvae to enter a developmentally slowed survival mode.

Limitations of the study

We were not able to directly assess iron levels, and so our interpretation of the rescue of slow growth by iron are indirect. We found that the *ftn-1p::GFP* reporter strain and Calcein AM dye did not respond to the iron levels in our experimental setup. Some of the experiments were carried out only as two biological replicates, as indicated in the figure legends.

STAR★METHODS

RESOURCE AVAILABILITY

Lead contact—Further information and requests for resources and reagents should be directed to and will be fulfilled by the lead author A.J.M. Walhout (marian.walhout@umassmed.edu).

Materials availability—All unique/stable reagents generated in this study are available from the lead contact without restriction.

Data and code availability

- RNA-seq data have been deposited at Gene Expression Omnibus (GEO): GSE and are publicly available as of the date of publication. Accession numbers: GSE213019 and GSE213057.
- This paper does not report original code.
- Any additional information required to reanalyze the data reported in this paper is available from the lead contact upon request.

EXPERIMENTAL MODEL AND STUDY PARTICIPANT DETAILS

C. elegans strains—*C. elegans* strains were maintained on nematode growth media and fed *E. coli* HB101.[4] N2 (Bristol) and VT1367 mals105 [*col19::GFP*] strains were used for developmental assays. The initial natural *P. aeruginosa* screen was performed with eggs, and other experiments were performed with synchronized L1s.

Bacterial strains—*E. coli* and *P. aeruginosa* strains were grown in Luria Bertani broth overnight at 37°C while shaking. CF18 transposon mutants were grown under the same conditions with the addition of 50 μg/mL gentamycin. *E. coli* BW25113 *fepG* mutant was grown with 50 μg/mL kanamycin.

METHOD DETAILS

Developmental phenotype assay (modified slow-killing culture conditions)—Bacterial strains were grown in Luria Bertani broth overnight at 37°C while shaking. 60 mm slow-killing plates (0.35% peptone, 1% NaCl, 0.25%, 50mM NaCl, 25mM [PO4], 5ug/mL Cholesterol, 1mM CaCl2, 1mM MgSO4, 1.5% Agarose) were seeded with 6 μL overnight cultures, covering the entire surface of the plate. Plates were incubated 24 h at 37°C and then 24 h at 25°C.

Bleached eggs were obtained by bleaching adult hermaphrodites, and synchronized L1s were obtained by incubating bleached eggs in M9 buffer overnight. Eggs or synchronized L1s were added to plates, and plates were maintained at 25°C for the duration of the assay. For each time point, the total number of animals in minimum of two plates and the total number of animals expressing *col19::GFP* were counted using a dissecting microscope. The percent of GFP positive animals were reported as percent adults in the graphs.

Adult lifespan assay—Eggs were obtained by bleaching hermaphrodite adult worms. Eggs were incubated in M9 buffer overnight to obtain synchronized L1 larvae. Synchronized L1 larvae were placed on nematode growth medium (NGM) plates seeded with HB101. After 48 h of incubation at 25°C, the young adult animals were collected and washed with M9 buffer 5 times. Slow-killing plates were prepared in the same manner as developmental assays. Young adult animals were seeded on SK plates with the indicated bacteria. At each time point, live and dead animals were counted. Animals were classified as dead when they no longer move and did not respond to 3 times gentle touch with a wire worm pick. For each time point, the percentage of animals alive in the plate was calculated and plotted. Experiments were carried out at 25°C.

Gut colonization assay—Ten to 20 animals fed bacteria were picked and anesthetized with 2% Triton X-100 and 60 mM sodium azide in M9. Then, animals were surface sterilized with 1/100 of bleaching solution for 5 min and washed 3 times with M9. Animals were re-counted and lysed using 0.5 mm glass beads. Lysates were serially diluted and plated on Luria-Bertani plates to calculate colony forming units (CFU) per animal. The last washing supernatant was plated as background control.

Transposon insertion library—The CF18 transposon insertion library was created as described by Kulasekara,[66] with some modifications. Briefly, CF18 was plated on LB plates and grown at 42°C overnight. The plasmid pBTK30 carrying hyperactive Himar1 C9 transposase was transferred to CF18 with bacterial conjugation using the *E. coli* SM10λpir strain at 1:8 bacterial ratio. After 1-h bacterial conjugation on LB plates, the bacteria were re-suspended and plated on LB + antibiotic plates. Gentamycin 50 mg/mL was used to select successful CF18 insertions and triclosan 25 μg/mL for counter selection of *E. coli*. The

next day, the single colonies were picked in a 96 well-plate containing LB with 50 μg/mL gentamycin and grown overnight. Glycerol was added to the plates at a final concentration of 25% and the libraries were stored in the −80°C freezer until further use.

CF18 transposon insertion library screen—Bacteria were grown at 37°C overnight in LB medium containing 50 μg/mL gentamycin. The 96-well plates containing SK media were seeded with 10 μL of overnight cultures and dried in the hood aseptically. Plates were incubated 1 day at 37°C then 1 day at 25°C. Gravid adults carrying *col-19::GFP* transgene were bleached to obtain eggs, and approximately 40 eggs were placed in each well of 96-well SK agar seeded with CF18 mutants. The experiment was performed in triplicate. Plates were incubated at 25°C and were scored under the fluorescence microscope for GFP positive animals on day 3 and day 5. The mutant bacteria that allowed larvae to reach adulthood on day 3 or 5 were subjected to a secondary testing with 60 mm SK plates for validation. Bacterial mutants with a confirmed attenuation profile in the secondary testing were genotyped to identify transposon insertion sites.

Genotyping CF18 mutants—Then, we identified the location of the transposon insertion by arbitrary PCR and sanger sequencing (Figure 2A). A two-step arbitrary PCR was performed on individual colonies as described by Kulasekara[66] using the primers in Table S6. PCR products were sequenced with Sanger sequencing, then sequences were blasted against the CF18 genome to determine the site and direction of the transposon insertion. For 2 intragenic insertions, we annotated each mutant with the gene name in which transposon was inserted; for the intergenic insertions, we used the first downstream gene name that was most likely affected by transposon insertion.

CF18 deletion mutants—Markerless deletion strains in CF18 background were created using the CRISPR-Cas9 based method by[74] with minor modifications. In brief, first, the plasmid-carrying Cas9 and lambda Red components was transformed into CF18 by electroporation. The guide targeting the gene to be deleted and the 1000 bp HR template were cloned into the pCRISPRPA plasmid. Cas9 expression was induced with 2 mg/mL L-arabinose overnight, then the second plasmid was transformed into CF18 by electroporation. Successful transformants were selected on LB plates with 50 μg/mL gentamycin and 100 μg/mL tetracycline. Colonies were screened for deletion by PCR and sanger sequencing. Plasmids were cured by negative selection on 5% sucrose media.

Bacterial growth rate—Overnight cultures of bacteria were serially diluted in LB in triplicate and grown for 30 h in 96 well-plates at 30°C on a Tecan Saphire plate reader. The OD600 nm measurements were recorded every 15 min. The $\log_{(10)}$OD values were plotted against time, and the growth rates(μ) were calculated using the exponential phase of the growth with the following formula: $OD_2 = OD_1 e^{\mu t}$, where OD1 is the OD600 measurement at the beginning of the exponential growth phase, OD2 is the OD600 value at the end of the exponential growth phase, and t is the duration of the exponential growth phase. The growth rates were normalized to the growth rate of WT CF18.

ROS detection with carboxy-H2DCFDA—Bacterial ROS measurements were performed using the fluorescent dye carboxy-H2DCFDA (Thermo Fisher Scientific) as

described by Zhang et al. 2019. The same dye was also used for ROS measurement in larvae. Briefly, the larvae were fed indicated bacteria for 24 h, then collected and washed with M9 five times. A stock solution of 10 mM carboxy-H2DCFDA was prepared in DMSO. The dye was added to the final concentration of 100 μM and incubated in the dark for 1 h at 25°C. After 5 times washing with M9, fluorescence in the larvae was detected using a Zeiss microscope with Axiovert camera. The same exposure time was used for all the experimental and control groups.

ROS detection with mitosox red—Larvae were incubated on slow-killing plates seeded with indicated bacteria for 24 h at 25°C, then collected and washed with M9 buffer. Mitosox Red dye solution was added to the final concentration of 10 μM. After 1 h incubation, the larvae were washed 5 times with M9 buffer. The experiments were conducted a minimum of two independent times with three replicates. Technical replicates were pooled before the microscopy. The first biological experiments were imaged using high magnification (63×) confocal microscopy. The second biological replicates were imaged with a lower magnification (20×) for quantification of fluorescence in whole animals. Images were obtained with a Leica SPE II microscope using the same gain settings for the experimental sets. The same brightness adjustments settings were applied to the whole images within the experimental sets with Leica LAS X software. For adult animals, anterior intestines were imaged as the mid-intestine was not observable due to the presence of embryos. We avoided using sterile strains lacking germline or L4 animals because it was previously reported that both the sterile animals and L4 stage animals are more resistant to *P. aeruginosa* than fertile and adult stage animals.[75]

TMRE assay—Slow killing plates were seeded with bacteria and incubated 24 h at 37°C. TMRE was added to the plates at the final concentration of 5 mM and plates were switched to 25°C. After 24 h of incubation at 25°C, synchronized L1 larvae were added to these plates. Plates were maintained at 25°C during the assay period. After 24 h of incubation, the larvae were collected by washing the plates with M9 buffer. Before microscopy, larvae were washed 5 times with M9 buffer to remove excess dye and bacteria. The experiments were conducted a minimum of two independent times with three technical replicates. Technical replicates were pooled before the microscopy. The first biological experiments were imaged using high magnification (63×) confocal microscopy. The second biological replicates were imaged with a lower magnification (20×) for quantification of fluorescence in whole animals. Images were taken on a confocal Leica SPE II microscope. Identical gain settings were used for the experimental sets. Image brightness levels were adjusted with Leica LAS X software and exact adjustments were applied to whole pictures within experimental sets. For adult animals, anterior intestines were imaged for the analysis.

Oxygen consumption rates—Oxygen consumption rates were measured using a Seahorse XFe96 Analyzer at room temperature as described previously with minor modifications.[69] In brief, synchronized L1 larvae were fed indicated bacteria for 1 to 4 h, then collected and washed 5 times with M9 buffer to remove excess bacteria. The number of animals in 1 μL of suspension was counted and adjusted. About 800 larvae were transferred per well of a 96-well microplate containing 180 μL M9 buffer. An equal volume of the

last M9 wash was also tested to monitor potential bacterial carry-over. Basal respiration was measured a total of 7 times that included a 2 min mix, a 5 min time delay, and a 2 min measurement. To measure maximum respiratory capacity, 15 μM carbonyl cyanide-4-(trifluoromethoxy) phenylhydrazone (FCCP) was injected and the oxygen consumption rate readings were repeated as basal respiration. Mitochondrial respiration was blocked by injecting 50 mM Sodium azide and measurements were repeated 7 times to estimate non-mitochondrial oxygen consumption. Five measurements before FCCP injection were used for baseline oxygen consumption; the maximum of 3 consecutive measurements were used for calculating maximum respiratory capacity; and the last two measurements were used for determining non-mitochondrial oxygen consumption. Non-mitochondrial oxygen consumption rates were deducted from the baseline and maximal oxygen consumption rates to calculate basal and maximal respiration. Each experiment was conducted with 6 replicates per condition and was repeated twice.

Quantification of microscopic images—Fluorescence measurements and size measurements of larvae were performed with Zen software and Fiji software from raw images. Data were normalized to mean fluorescence intensity of *gacA*-fed larvae for Mitosox Red and TMRE measurements. Prism 8 (Graphpad) was used to determine DT50 values.

RNA-sequencing—Larvae fed CF18 and CF18 *gacA* mutant were collected after 4 and 6 h and washed three times with M9 buffer. Samples were frozen in liquid nitrogen, and the total RNA was isolated with the TRIZOL method.

Ribosomal RNA was depleted with an antisense DNA oligo and RNAse-H based method as described in a previous study.[76] The libraries were prepared with the NebNext Ultra II non directional kit (NEB, Cat: E7775, E7335, E7500), according to the manufacturer's instructions. The libraries were pooled and sequenced with the Illumina NextSeq 500 system.

RNA-sequencing data analysis—Cutadapt/1.4.1 was used to trim adaptor sequences and filter out the reads shorter than 15 nt.[77] The reads were mapped to the *C. elegans* genome (Wbcel235) by Star/2.5.3 aligner.[78] Samtools/1.9 was used for sorting data, and gene counts were obtained with Featurecounts.[79,80] Differential gene expression analysis was performed with DEBrowser.[81] For *C. elegans* data, data was normalized by median ratio normalization (MRN) and batch effects were corrected with the ComBat method, which are built in the DEBrowser. We used a fold change of 2 and *p* adjusted value of smaller than 0.01 as cutoffs for determining differentially expressed genes.

The Gene Ontology Term Analysis was performed using WormCat and DAVID.[34,35]

RNAi treatment—RNAi by feeding experiments were performed as described by Kamath et al. 2001.[82] Briefly, the RNAi screen was performed by seeding individual RNAi clones onto 60 mm NGM plates containing 1 mM Isopropyl β-D-thiogalactopyranoside (IPTG) and 50 mg/mL ampicillin. Dried plates were kept at 20°C overnight to induce the expression of

dsRNAs. Synchronized L1 N2 animals were raised on the RNAi plates at 25°C for 24 h. Then, animals were collected, and the ROS levels were assessed with Mitosox Red stain.

Calcium and magnesium measurements—Calcium measurements were performed with *C. elegans (zcIs17)*. Larvae were incubated on slow-killing plates seeded with the indicated bacteria for 24 h at 25°C, then collected and washed with M9 buffer. Rhodamine 2 a.m. or Magnesium Green AM dyes were added to the final concentration of 5 μM. After 1 h incubation, the larvae were washed 5 times with M9 buffer. Images were taken with a Leica SPE II microscope. The same brightness adjustments settings were applied to the whole images within the experimental sets with Leica LAS X software. Quantification of fluorescence intensities was performed with Zen Blue and Fiji, using raw images; intestinal tracts were omitted.

EMS and ENU mutagenesis—Synchronized L4 hermaphrodite animals carrying the *col-19::GFP* transgene were washed three times with M9 buffer to remove bacteria. Then, the EMS and ENU solution (final concentration of 50mM and 1mM respectively) was added. The animals were incubated for 4 h while shaking at 20°C. The mutagenized animals were washed five times with M9 and were placed onto NGM plates seeded with HB101. They were then incubated until the F1 progeny reached adulthood. The F1 animals were bleached to obtain synchronized L1 stage F2 eggs. The F2 progeny was scored on CF18-seeded plates for *col-19::GFP* expression at 48 and 72-h time points. The mutagenesis screen was repeated two times.

QUANTIFICATION AND STATISTICAL ANALYSIS

Statistical analyses were performed using one-way ANOVA, followed multiple comparison tests with the Bonferroni adjustment, using GraphPad Prism versions 9 and 10. The equality of standard deviations between the samples was assessed using the Bartlett test. In cases of unequal standard deviations, statistical comparisons were conducted using Welch-style ANOVA followed by Dunnett's T3 adjustment for multiple comparisons. For single comparisons, we conducted a two-tailed Student's *t*-test. Data are represented as the mean ± SD of independent experiments, as indicated in the figure legends. Adjusted p values (p_{adj}) < 0.05 were considered statistically significant.

Supplementary Material

Refer to Web version on PubMed Central for supplementary material.

ACKNOWLEDGMENTS

We thank Alejandro Vasquez Rifo for assessing the lifespan of adult animals with natural *P. aeruginosa* strains, Amy Walker for providing access to the confocal microscope, and John Haley and David A. Guertin for guidance with Seahorse measurements. We also thank the members of Walhout and Ambros lab for discussions and Caryn Navarro for help in editing this manuscript. Some of the nematode strains were provided by the Caenorhabditis Genetics Center, which is funded by the NIH Office of Research Infrastructure Programs (P40 OD010440). This research was supported by funding from NIH grants R35GM122502 (to A.J.M.W.), R01DK068429 (to A.J.M.W.), R01GM104904 (to A.J.M.W. and V.A.), R01GM034028 (to V.A.), and R35GM131741 (to V.A.).

REFERENCES

1. Glynn JR, and Moss PAH (2020). Systematic analysis of infectious disease outcomes by age shows lowest severity in school-age children. Sci. Data 7, 329. 10.1038/s41597-020-00668-y. [PubMed: 33057040]
2. Simon AK, Hollander GA, and McMichael A. (2015). Evolution of the immune system in humans from infancy to old age. Proc. Biol. Sci 282, 20143085. 10.1098/rspb.2014.3085.
3. Sulston JE, and Horvitz HR (1977). Post-embryonic cell lineages of the nematode, Caenorhabditis elegans. Dev. Biol 56, 110–156. 10.1016/0012-1606(77)90158-0. [PubMed: 838129]
4. Brenner S. (1974). The genetics of Caenorhabditis elegans. Genetics 77, 71–94. [PubMed: 4366476]
5. Byerly L, Cassada RC, and Russell RL (1976). The life cycle of the nematode Caenorhabditis elegans. Dev. Biol 51, 23–33. 10.1016/0012-1606(76)90119-6. [PubMed: 988845]
6. Macneil LT, and Walhout AJ (2013). Food, pathogen, signal: The multifaceted nature of a bacterial diet. Worm 2, e26454. 10.4161/worm.26454. [PubMed: 24744980]
7. Samuel BS, Rowedder H, Braendle C, Fé lix MA, and Ruvkun G. (2016). Caenorhabditis elegans responses to bacteria from its natural habitats. Proc. Natl. Acad. Sci. USA 113, E3941–E3949. 10.1073/pnas.1607183113. [PubMed: 27317746]
8. Shtonda BB, and Avery L. (2006). Dietary choice behavior in Caenorhabditis elegans. J. Exp. Biol 209, 89–102. 10.1242/jeb.01955. [PubMed: 16354781]
9. Kim DH, Feinbaum R, Alloing G, Emerson FE, Garsin DA, Inoue H, Tanaka-Hino M, Hisamoto N, Matsumoto K, Tan MW, and Ausubel FM (2002). A Conserved p38 MAP Kinase Pathway in Caenorhabditis elegans Innate Immunity. Science 297, 623–626. 10.1126/science.1073759. [PubMed: 12142542]
10. Nhan JD, Turner CD, Anderson SM, Yen CA, Dalton HM, Cheesman HK, Ruter DL, Uma Naresh N, Haynes CM, Soukas AA, et al. (2019). Redirection of SKN-1 abates the negative metabolic outcomes of a perceived pathogen infection. Proc. Natl. Acad. Sci. USA 116, 22322–22330. 10.1073/pnas.1909666116. [PubMed: 31611372]
11. Anderson SM, and Pukkila-Worley R. (2020). Immunometabolism in caenorhabditis elegans. PLoS Pathog. 16, e1008897. 10.1371/journal.ppat.1008897.
12. Lobet E, Letesson JJ, and Arnould T. (2015). Mitochondria: A target for bacteria. Biochem. Pharmacol 94, 173–185. 10.1016/j.bcp.2015.02.007. [PubMed: 25707982]
13. Miranda-Vizuete A, and Veal EA (2017). Caenorhabditis elegans as a model for understanding ROS function in physiology and disease. Redox Biol. 11, 708–714. 10.1016/j.redox.2016.12.020. [PubMed: 28193593]
14. Anderson CP, and Leibold EA (2014). Mechanisms of iron metabolism in caenorhabditis elegans. Front. Pharmacol 5, 113–118. 10.3389/fphar.2014.00113. [PubMed: 24904417]
15. Dixon SJ, and Stockwell BR (2014). The role of iron and reactive oxygen species in cell death. Nat. Chem. Biol 10, 9–17. 10.1038/nchembio.1416. [PubMed: 24346035]
16. Valentini S, Cabreiro F, Ackerman D, Alam MM, Kunze MBA, Kay CWM, and Gems D. (2012). Manipulation of in vivo iron levels can alter resistance to oxidative stress without affecting ageing in the nematode C. elegans. Mech. Ageing Dev. 133, 282–290. 10.1016/j.mad.2012.03.003. [PubMed: 22445852]
17. Zhang J, Li X, Olmedo M, Holdorf AD, Shang Y, Artal-Sanz M, Yilmaz LS, and Walhout AJM (2019). A Delicate Balance between Bacterial Iron and Reactive Oxygen Species Supports Optimal C. elegans Development. Cell Host Microbe 26, 400–411.e3. 10.1016/j.chom.2019.07.010. [PubMed: 31444089]
18. Nargund AM, Pellegrino MW, Fiorese CJ, Baker BM, and Haynes CM (2012). Mitochondrial Import Efficiency of. Science 337, 587–590. 10.1126/science.1223560. [PubMed: 22700657]
19. Shpilka T, and Haynes CM (2018). The mitochondrial UPR: Mechanisms, physiological functions and implications in ageing. Nat. Rev. Mol. Cell Biol 19, 109–120. 10.1038/nrm.2017.110. [PubMed: 29165426]
20. Pellegrino MW, Nargund AM, Kirienko NV, Gillis R, Fiorese CJ, and Haynes CM (2014). Mitochondrial UPR-regulated innate immunity provides resistance to pathogen infection. Nature 516, 414–417. 10.1038/nature13818. [PubMed: 25274306]

21. Pearson JP, Feldman M, Iglewski BH, and Prince A. (2000). Pseudomonas aeruginosa cell-to-cell signaling is required for virulence in a model of acute pulmonary infection. Infect. Immun 68, 4331–4334. 10.1128/IAI.68.7.4331-4334.2000. [PubMed: 10858254]
22. Moradali MF, Ghods S, and Rehm BHA (2017). Pseudomonas aeruginosa lifestyle: A paradigm for adaptation, survival, and persistence. Front. Cell. Infect. Microbiol 7, 39. 10.3389/fcimb.2017.00039. [PubMed: 28261568]
23. Hall S, McDermott C, Anoopkumar-Dukie S, McFarland AJ, Forbes A, Perkins AV, Davey AK, Chess-Williams R, Kiefel MJ, Arora D, and Grant GD (2016). Cellular effects of pyocyanin, a secreted virulence factor of Pseudomonas aeruginosa. Toxins 8, 236. 10.3390/toxins8080236.
24. Blumer C, and Haas D. (2000). Mechanism, regulation, and ecological role of bacterial cyanide biosynthesis. Arch. Microbiol 173, 170–177. 10.1007/s002039900127. [PubMed: 10763748]
25. Mahajan-Miklos S, Tan MW, Rahme LG, and Ausubel FM (1999). Molecular mechanisms of bacterial virulence elucidated using a Pseudomonas aeruginosa-Caenorhabditis elegans pathogenesis model. Cell 96, 47–56. 10.1016/S0092-8674(00)80958-7. [PubMed: 9989496]
26. Cooper CE, and Brown GC (2008). The inhibition of mitochondrial cytochrome oxidase by the gases carbon monoxide, nitric oxide, hydrogen cyanide and hydrogen sulfide: Chemical mechanism and physiological significance. J. Bioenerg. Biomembr 40, 533–539. 10.1007/s10863-008-9166-6. [PubMed: 18839291]
27. Vasquez-Rifo A, Veksler-Lublinsky I, Cheng Z, Ausubel FM, and Ambros V. (2019). The Pseudomonas aeruginosa accessory genome elements influence virulence towards Caenorhabditis elegans. Genome Biol. 20, 270. 10.1186/s13059-019-1890-1. [PubMed: 31823826]
28. Blelloch R, Anna-Arriola SS, Gao D, Li Y, Hodgkin J, and Kimble J. (1999). The gon-1 gene is required for gonadal morphogenesis in Caenorhabditis elegans. Dev. Biol 216, 382–393. 10.1006/dbio.1999.9491. [PubMed: 10588887]
29. Gritti N, Kienle S, Filina O, and Van Zon JS (2016). Long-term timelapse microscopy of C. Elegans post-embryonic development. Nat. Commun 7, 12500. 10.1038/ncomms12500. [PubMed: 27558523]
30. Harfe BD, Vaz Gomes A, Kenyon C, Liu J, Krause M, and Fire A. (1998). Analysis of a Caenorhabditis elegans twist homolog identifies conserved and divergent aspects of mesodermal patterning. Genes Dev. 12, 2623–2635. 10.1101/gad.12.16.2623. [PubMed: 9716413]
31. Fielenbach N, and Antebi A. (2008). C. elegans dauer formation and the molecular ba1. S. Y. Park, M. Tong, and J. L. Jameson. Genes Dev. 22, 2149–2165. 10.1101/gad.1701508.
32. Tan MW, Mahajan-Miklos S, and Ausubel FM (1999). Killing of Caenorhabditis elegans by Pseudomonas aeruginosa used to model mammalian bacterial pathogenesis. Proc. Natl. Acad. Sci. USA 96, 715–720. 10.1073/pnas.96.2.715. [PubMed: 9892699]
33. Rahme LG, Stevens EJ, Wolfort SF, Shao J, Tompkins RG, and Ausubel FM (1995). Common virulence factors for bacterial pathogenicity in plants and animals. Science 268, 1899–1902. 10.1126/science.7604262. [PubMed: 7604262]
34. Huang DW, Sherman BT, and Lempicki RA (2009). Systematic and integrative analysis of large gene lists using DAVID bioinformatics resources. Nat. Protoc 4, 44–57. 10.1038/nprot.2008.211. [PubMed: 19131956]
35. Holdorf AD, Higgins DP, Hart AC, Boag PR, Pazour GJ, Walhout AJM, and Walker AK (2020). WormCat: An online tool for annotation and visualization of caenorhabditis elegans genome-scale data. Genetics 214, 279–294. 10.1534/genetics.119.302919. [PubMed: 31810987]
36. Troemel ER, Chu SW, Reinke V, Lee SS, Ausubel FM, and Kim DH (2006). p38 MAPK regulates expression of immune response genes and contributes to longevity in C. elegans. PLoS Genet. 2, e183–e1739. 10.1371/journal.pgen.0020183. [PubMed: 17096597]
37. Tepper RG, Ashraf J, Kaletsky R, Kleemann G, Murphy CT, and Bussemaker HJ (2013). PQM-1 Complements DAF-16 as a Key Transcriptional Regulator of DAF-2-Mediated Development and Longevity. Cell 154, 676–690. 10.1016/j.cell.2013.07.006. [PubMed: 23911329]
38. Sarasija S, and Norman KR (2018). Analysis of Mitochondrial Structure in the Body Wall Muscle of Caenorhabditis elegans. Bio. Protoc 8, e2801–e2815. 10.21769/BioProtoc.2801.

39. Scaduto RC, and Grotyohann LW (1999). Measurement of mitochondrial membrane potential using fluorescent rhodamine derivatives. Biophys. J 76, 469–477. 10.1016/S0006-3495(99)77214-0. [PubMed: 9876159]
40. Zorova LD, Popkov VA, Plotnikov EY, Silachev DN, Pevzner IB, Jankauskas SS, Babenko VA, Zorov SD, Balakireva AV, Juhaszova M, et al. (2018). Mitochondrial membrane potential. Anal. Biochem 552, 50–59. 10.1016/j.ab.2017.07.009. [PubMed: 28711444]
41. Yee C, Yang W, and Hekimi S. (2014). The intrinsic apoptosis pathway mediates the pro-longevity response to mitochondrial ROS in C elegans. Cell 157, 897–909. 10.1016/j.cell.2014.02.055. [PubMed: 24813612]
42. Dingley S, Polyak E, Lightfoot R, Ostrovsky J, Rao M, Greco T, Ischiropoulos H, and Falk MJ (2010). Mitochondrial respiratory chain dysfunction variably increases oxidant stress in Caenorhabditis elegans. Mitochondrion 10, 125–136. 10.1016/j.mito.2009.11.003. [PubMed: 19900588]
43. Melo JA, and Ruvkun G. (2012). Inactivation of conserved C. elegans genes engages pathogen- and xenobiotic-associated defenses. Cell 149, 452–466. 10.1016/j.cell.2012.02.050. [PubMed: 22500807]
44. Kamath RS, Fraser AG, Dong Y, Poulin G, Durbin R, Gotta M, Kanapin A, Le Bot N, Moreno S, Sohrmann M, et al. (2003). Systematic functional analysis of the Caenorhabditis elegans genome using RNAi. Nature 421, 231–237. 10.1038/nature01278. [PubMed: 12529635]
45. Yoneda T, Benedetti C, Urano F, Clark SG, Harding HP, and Ron D. (2004). Compartment-specific perturbation of protein handling activates genes encoding mitochondrial chaperones. J. Cell Sci. 117, 4055–4066. 10.1242/jcs.01275. [PubMed: 15280428]
46. Honda Y, and Honda S. (1999). The daf-2 gene network for longevity regulates oxidative stress resistance and Mn-superoxide dismutase gene expression in Caenorhabditis elegans. Faseb. J 13, 1385–1393. 10.1096/fasebj.13.11.1385. [PubMed: 10428762]
47. Deng P, Uma Naresh N, Du Y, Lamech LT, Yu J, Zhu LJ, Pukkila-Worley R, and Haynes CM (2019). Mitochondrial UPR repression during Pseudomonas aeruginosa infection requires the bZIP protein ZIP-3. Proc. Natl. Acad. Sci. USA 116, 6146–6151. 10.1073/pnas.1817259116. [PubMed: 30850535]
48. Govindan JA, Jayamani E, and Ruvkun G. (2019). ROS-based lethality of Caenorhabditis elegans mitochondrial electron transport mutants grown on Escherichia coli siderophore iron release mutants. Proc. Natl. Acad. Sci. USA 116, 21651–21658. 10.1073/pnas.1912628116. [PubMed: 31591219]
49. Levi S, and Rovida E. (2009). The role of iron in mitochondrial function. Biochim. Biophys. Acta 1790, 629–636. 10.1016/j.bbagen.2008.09.008. [PubMed: 18948172]
50. Di Monte D, Sandy MS, Ekströ m G, and Smith MT (1986). Comparative studies on the mechanisms of paraquat and 1-methyl-4-phenylpyridine (MPP+) cytotoxicity. Biochem. Biophys. Res. Commun 137, 303–309. 10.1016/0006-291X(86)91210-6. [PubMed: 3487318]
51. Lee SJ, Hwang AB, and Kenyon C. (2010). Inhibition of respiration extends C. elegans life span via reactive oxygen species that increase HIF-1 activity. Curr. Biol 20, 2131–2136. 10.1016/j.cub.2010.10.057. [PubMed: 21093262]
52. Zhao Z. (2019). Iron and oxidizing species in oxidative stress and Alzheimer's disease. Aging Med. 2, 82–87. 10.1002/agm2.12074.
53. Daw CC, Ramachandran K, Enslow BT, Maity S, Bursic B, Novello MJ, Rubannelsonkumar CS, Mashal AH, Ravichandran J, Bakewell TM, et al. (2020). Lactate Elicits ER-Mitochondrial Mg2+ Dynamics to Integrate Cellular Metabolism. Cell 183, 474–489.e17. 10.1016/j.cell.2020.08.049. [PubMed: 33035451]
54. Mallilankaraman K, Doonan P, Cá rdenas C, Chandramoorthy HC, Müller M, Miller R, Hoffman NE, Gandhirajan RK, Molgo J, Birnbaum MJ, et al. (2012). MICU1 is an essential gatekeeper for mcu-mediated mitochondrial Ca 2+ uptake that regulates cell survival. Cell 151, 630–644. 10.1016/j.cell.2012.10.011. [PubMed: 23101630]
55. Madaris TR, Venkatesan M, Maity S, Stein MC, Vishnu N, Venkateswaran MK, Davis JG, Ramachandran K, Uthayabalan S, Allen C, et al. (2023). Limiting Mrs2-dependent mitochondrial

Mg2+ uptake induces metabolic programming in prolonged dietary stress. Cell Rep. 42, 112155. 10.1016/j.celrep.2023.112155. [PubMed: 36857182]

56. Briard B, Bomme P, Lechner BE, Mislin GLA, Lair V, Prévost MC, Latgé JP, Haas H, and Beauvais A. (2015). Pseudomonas aeruginosa manipulates redox and iron homeostasis of its microbiota partner Aspergillus fumigatus via phenazines. Sci. Rep 5, 8220. 10.1038/srep08220. [PubMed: 25665925]
57. Managò A, Becker KA, Carpinteiro A, Wilker B, Soddemann M, Seitz AP, Edwards MJ, Grassmé H, Szabò I, and Gulbins E. (2015). Pseudomonas aeruginosa Pyocyanin Induces Neutrophil Death via Mitochondrial Reactive Oxygen Species and Mitochondrial Acid Sphingomyelinase. Antioxid. Redox Signal. 22, 1097–1110. 10.1089/ars.2014.5979. [PubMed: 25686490]
58. Higgins S, Heeb S, Rampioni G, Fletcher MP, Williams P, and Cámara M. (2018). Differential regulation of the phenazine biosynthetic operons by quorum sensing in Pseudomonas aeruginosa PAO1-N. Front. Cell. Infect. Microbiol 8, 252. 10.3389/fcimb.2018.00252. [PubMed: 30083519]
59. Reimmann C, Beyeler M, Latifi A, Winteler H, Foglino M, Lazdunski A, and Haas D. (1997). The global activator GacA of Pseudomonas aeruginosa PAO positively controls the production of the autoinducer N-butyryl-homoserine lactone and the formation of the virulence factors pyocyanin, cyanide, and lipase. Mol. Microbiol 24, 309–319. 10.1046/j.1365-2958.1997.3291701.x. [PubMed: 9159518]
60. Schalk IJ, and Perraud Q. (2023). Pseudomonas aeruginosa and its multiple strategies to access iron. Environ. Microbiol 25, 811–831. 10.1111/1462-2920.16328. [PubMed: 36571575]
61. Chen L, Zou Y, She P, and Wu Y. (2015). Composition, function, and regulation of T6SS in Pseudomonas aeruginosa. Microbiol. Res 172, 19–25. 10.1016/j.micres.2015.01.004. [PubMed: 25721475]
62. Cianfanelli FR, Monlezun L, and Coulthurst SJ (2016). Aim, Load, Fire: The Type VI Secretion System, a Bacterial Nanoweapon. Trends Microbiol. 24, 51–62. 10.1016/j.tim.2015.10.005. [PubMed: 26549582]
63. Gallagher LA, and Manoil C. (2001). Pseudomonas aeruginosa PAO1 kills Caenorhabditis elegans by cyanide poisoning. J. Bacteriol 183, 6207–6214. 10.1128/JB.183.21.6207. [PubMed: 11591663]
64. Way JL (1984). Cyanide Intoxication and its Mechanism of Antagonism. Annu. Rev. Pharmacol. Toxicol 24, 451–481. 10.1146/an-nurev.pa.24.040184.002315. [PubMed: 6428300]
65. Leavesley HB, Li L, Prabhakaran K, Borowitz JL, and Isom GE (2008). Interaction of cyanide and nitric oxide with cytochrome c oxidase: Implications for acute cyanide toxicity. Toxicol. Sci 101, 101–111. 10.1093/toxsci/kfm254. [PubMed: 17906319]
66. Kulasekara HD (2014). Transposon Mutagenesis. In Methods in Molecular Biology, pp. 501–519. 10.1007/978-1-4939-0473-0_39.
67. Liu Z, Kirch S, and Ambros V. (1995). The Caenorhabditis elegans heterochronic gene pathway controls stage-specific transcription of collagen genes. Development 121, 2471–2478. 10.1242/dev.121.8.2471. [PubMed: 7671811]
68. Feinbaum RL, Urbach JM, Liberati NT, Djonovic S, Adonizio A, Carvunis AR, and Ausubel FM (2012). Genome-wide identification of Pseudomonas aeruginosa virulence-related genes using a Caenorhabditis elegans infection model. PLoS Pathog. 8, e1002813. 10.1371/journal.ppat.1002813.
69. Jimenez PN, Koch G, Thompson JA, Xavier KB, Cool RH, and Quax WJ (2012). The Multiple Signaling Systems Regulating Virulence in Pseudomonas aeruginosa. Microbiol. Mol. Biol. Rev 76, 46–65. 10.1128/mmbr.05007-11. [PubMed: 22390972]
70. Klockgether J, Cramer N, Wiehlmann L, Davenport CF, and Tümmler B. (2011). Pseudomonas aeruginosa genomic structure and diversity. Front. Microbiol 2, 150. 10.3389/fmicb.2011.00150. [PubMed: 21808635]
71. Liu Y, Samuel BS, Breen PC, and Ruvkun G. (2014). Caenorhabditis elegans pathways that surveil and defend mitochondria. Nature 508, 406–410. 10.1038/nature13204. [PubMed: 24695221]
72. Deng P, Uma Naresh N, Du Y, Lamech LT, Yu J, Zhu LJ, Pukkila-Worley R, and Haynes CM (2019). Mitochondrial UPR repression during Pseudomonas aeruginosa infection requires the bZIP

protein ZIP-3. Proc. Natl. Acad. Sci. USA 116, 6146–6151. 10.1073/pnas.1817259116. [PubMed: 30850535]

73. Schindelin J, Arganda-Carreras I, Frise E, Kaynig V, Longair M, Pietzsch T, Preibisch S, Rueden C, Saalfeld S, Schmid B, et al. (2012). Fiji: An open-source platform for biological-image analysis. Nat. Methods 9, 676–682. 10.1038/nmeth.2019. [PubMed: 22743772]
74. Chen W, Zhang Y, Zhang Y, Pi Y, Gu T, Song L, Wang Y, and Ji Q. (2018). CRISPR/Cas9-based Genome Editing in Pseudomonas aeruginosa and Cytidine Deaminase-Mediated Base Editing in Pseudomonas Species. iScience 6, 222–231. 10.1016/j.isci.2018.07.024. [PubMed: 30240613]
75. Tekippe M, and Aballay A. (2010). C. elegans germline-deficient mutants respond to pathogen infection using shared and distinct mechanisms. PLoS One 5, e11777. 10.1371/journal.pone.0011777. [PubMed: 20668681]
76. Duan Y, Sun Y, and Ambros V. (2020). RNA-seq with RNase H-based ribosomal RNA depletion specifically designed for C. elegans. MicroPubl. Biol 2020, 22–25. 10.17912/micropub.biology.000312.
77. Martin M. (2011). Cutadapt removes adapter sequences from highthroughput sequencing reads. EMBnet. j 17, 10. 10.14806/ej.17.1.200.
78. Dobin A, Davis CA, Schlesinger F, Drenkow J, Zaleski C, Jha S, Batut P, Chaisson M, and Gingeras TR (2013). STAR: Ultrafast universal RNA-seq aligner. Bioinformatics 29, 15–21. 10.1093/bioinformatics/bts635. [PubMed: 23104886]
79. Li H, Handsaker B, Wysoker A, Fennell T, Ruan J, Homer N, Marth G, Abecasis G, and Durbin R; 1000 Genome Project Data Processing Subgroup (2009). The Sequence Alignment/Map format and SAMtools. Bioinformatics 25, 2078–2079. 10.1093/bioinformatics/btp352.
80. Liao Y, Smyth GK, and Shi W. (2014). FeatureCounts: An efficient general purpose program for assigning sequence reads to genomic features. Bioinformatics 30, 923–930. 10.1093/bioinformatics/btt656. [PubMed: 24227677]
81. Kucukural A, Yukselen O, Ozata DM, Moore MJ, and Garber M. (2019). DEBrowser: interactive differential expression analysis and visualization tool for count data. BMC Genom. 20, 6–12. 10.1186/s12864-018-5362-x.
82. Kamath RS, Martinez-Campos M, Zipperlen P, Fraser AG, and Ahringer J. (2001). Effectiveness of specific RNA-mediated interference through ingested double-stranded RNA in Caenorhabditis elegans. Genome Biol. 2, RESEARCH0002.

Highlights

- *P. aeruginosa* CF18 causes extreme but reversible growth delay in *C. elegans* larvae
- Mitochondrial dysfunction because of high ROS and iron imbalance causes slow growth
- While UPR^{mt} is inhibited, mitophagy is required for survival
- QS and GacA/S-regulated non-phenazine toxins cause developmental slowing

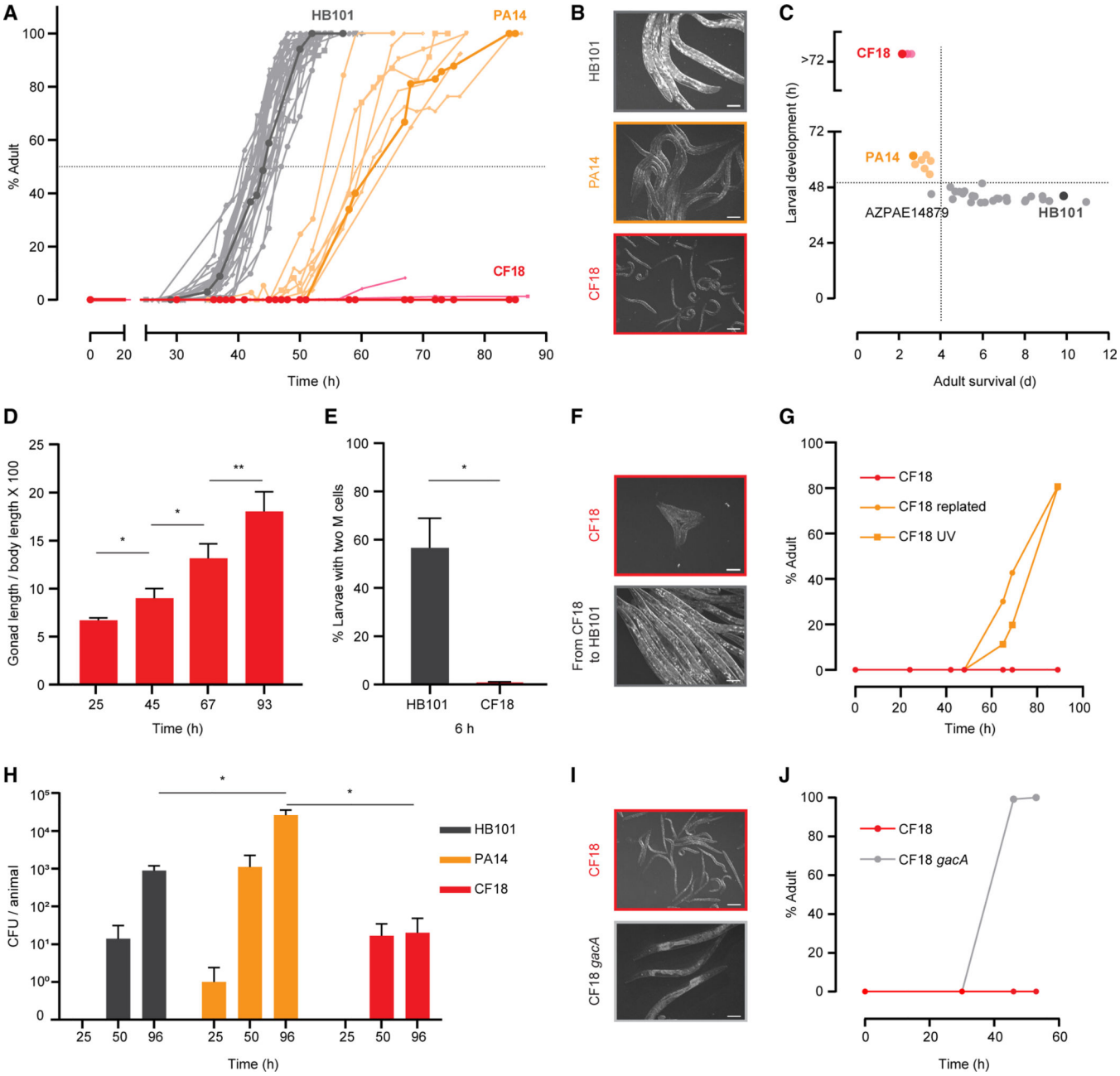

Figure 1. CF18 causes the most severe developmental slowing of *C. elegans* larvae among 36 natural *P. aeruginosa* strains

(A) Time of development to adulthood of *C. elegans* fed 36 *P aeruginosa* strains, PA14 *gacA* mutant, and *Escherichia coli* HB101. Normal, moderately slow, and slow colored as gray, orange, and red, respectively. Experiments were set up with bleached eggs. Two biological replicates were combined for the graph. See also Table S1).

(B) Representative bright-field images of *C. elegans* larvae fed HB101, PA14, or CF18 at 48 h.

(C)Larval development and adult survival profiles. Larval developmental times refer to the time (hours) when 50% of the larvae reached the adult stage (A). CF18-, WC55-, and

AZPAE15026-fed larvae did not reach the adult stage, so values are plotted as greater than 72 h. Adult survival data are from separate adult killing assays.

(D) The gonad length to worm length ratio of CF18-fed larvae increases over time, reflecting developmental progression (albeit slow). Data are shown as means of three biological replicates ± standard deviation (SD). **the p value adjusted for multiple comparisons (p_{adj})< 0.01, *p_{adj} < 0.05 (one-way ANOVA with Bonferroni correction). See also Figure S1B.

(E) The percentage of animals that completed the first division of the M cell lineage (visualized using *Phlh-8::GFP*) at 6 h. Data are represented as means of two biological replicates ± SD. *p < 0.05 (t test).

(F) CF18-fed larvae can resume development after being transferred to non-pathogenic bacteria. Synchronized L1 animals were exposed to CF18 for 3 days and then transferred to HB101. Images were captured after 48 h on HB101.

(G) Developmental slowing by CF18 requires bacterial secreted compounds and active bacterial metabolism. For all conditions, bacterial lawns were grown for 48 h and then UV irradiated (0.15 J), transferred to a fresh plate, or left untreated. Then the plates were inoculated with L1s, and the time to reach adulthood was monitored.

(H) The intestine was not colonized by bacteria in larvae fed CF18. Data are represented as means of two replicates ± SD. *p_{adj} < 0.05 (one-way ANOVA with Bonferroni correction).

(I) CF18 *gacA*-fed larvae exhibited a normal developmental rate. Shown are microscopy images of larvae fed WT CF18 or CF18 *gacA* at 48 h.

(J) Developmental graphs of WT CF18- and CF18 *gacA*-fed larvae.

Representative developmental graphs (G and J) and images (B, F, and I) are from a minimum of three biological replicates. Scale bars, 100 μm.

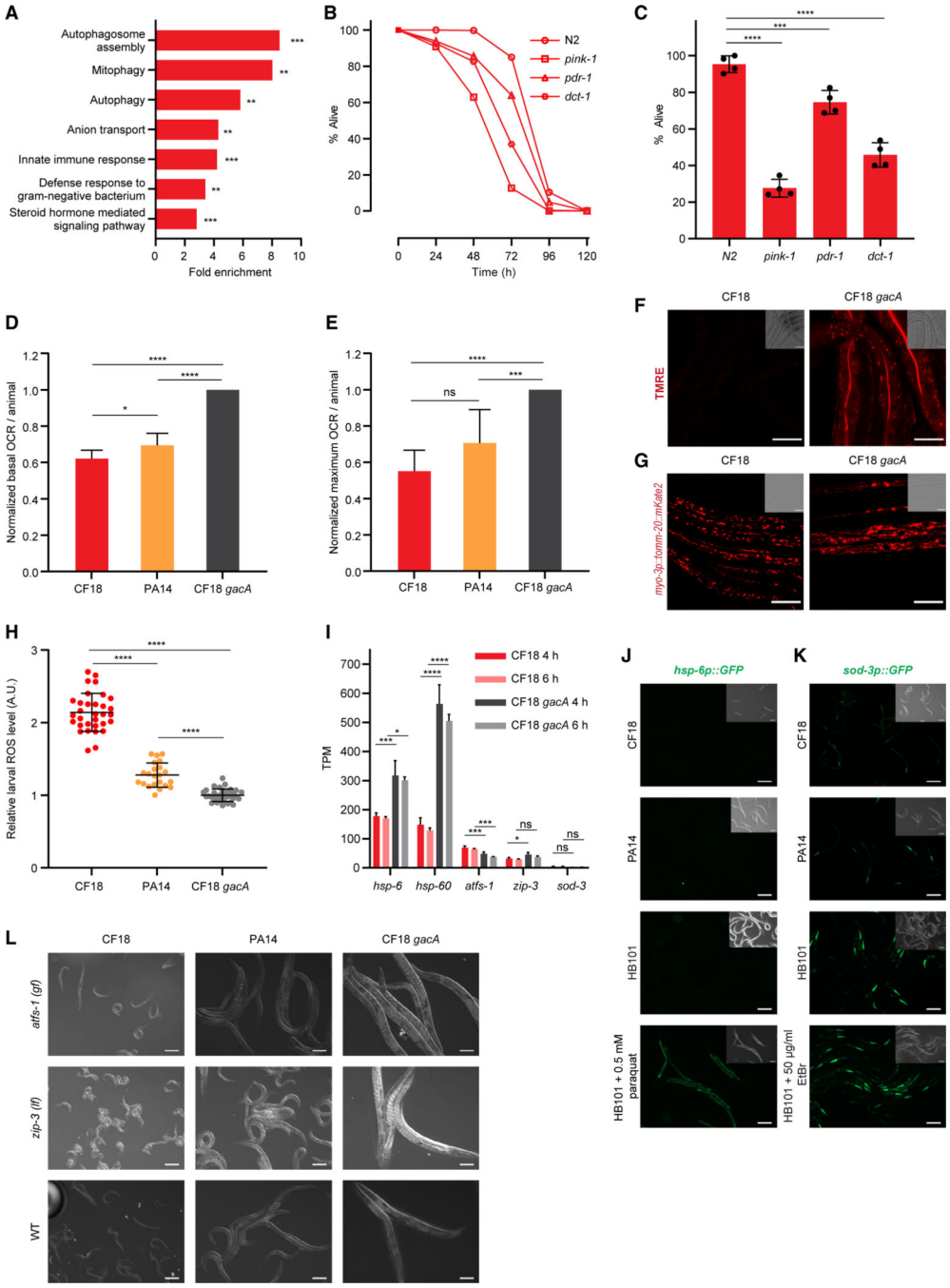

Figure 2. Larvae fed CF18 exhibit mitochondrial dysfunction and high ROS levels, yet UPR^{mt} is not activated

(A) Gene Ontology (GO) enrichment analysis of genes upregulated in 4-h CF18-fed larvae in comparison with 4-h *gacA*-fed larvae. Three biological replicates. Benjamini, p_{adj} values: ***$p < 0.001$, **$p < 0.01$. Genes were considered upregulated when $p_{adj} < 0.01$ and $\log_2$ fold change ≥ 1.

(B) Mitophagy mutants survive for a shorter time on CF18 than WT animals. For each strain, 180–279 animals were analyzed. Two replicates.

(C) Animals were transferred to non-pathogenic *E. coli* HB101 after 48 h of CF18 exposure. Recovery is impaired in mitophagy mutants. Mean and SD of the 4 replicates are shown for each strain. The total of animals is 336, 538, 611, and 570 for the N2, *pink-1*, *dct-1*, and *pdr-1* strains, respectively.

(D) CF18- or PA14-fed larvae exhibited a decreased basal OCR at 4 h. Data are shown as means of 6 biological experiments ± SD.

(E) Maximum OCR rates of CF18-, PA14-, or CF18-fed larvae at 4 h. Data are shown as means of 6 biological experiments ± SD.

(F) TMRE staining shows that the ΔΨm was disrupted in CF18-fed larvae. Representative midgut confocal images of three biological replicates are shown. Scale bars, 25 μm.

(G) The mitochondrial network of body wall muscle in CF18-fed larvae was fragmented. Transgenic animals carrying the mitochondrial marker *Pmyo-3::tomm-20::mKate2* were exposed to CF18 and *gacA* for 24 h. Representative confocal images of two biological replicates are shown. Scale bars, 25 μm.

(H) Quantification of MitoSOX Red staining showed that larvae fed CF18 have high levels of ROS. PA14 had intermediate levels of ROS. Error bars indicate ±SD. For each condition, 22–35 animals were quantified. ****$p_{adj} < 0.0001$ (Welch's ANOVA with Dunnett's T3 correction).

(I) UPR^{mt} was not induced in larvae exposed to CF18 for 4 h. Shown are transcript per million (TPM) values of the UPR^{mt}-related chaperones *hsp-6*, *hsp-60*, transcription factor ATFS-1, UPR^{mt} repressor *zip-3* and mitochondrial superoxide dismutase *sod-3*. Mean ± SD of three biological replicates.

(J) CF18-fed larvae did not induce *Phsp-6::GFP* expression after 28 h of feeding. HB101 with 0.5 mM paraquat was used as the positive control. Representative images of three biological replicates are shown.

(K) *sod-3* was not induced in CF18-fed animals. Microscopy images of transgenic animals carrying *Psod-3::GFP* were taken after 28 h of exposure. Representative images of three biological replicates are shown.

(L) Microscopy images showing developmental phenotypes of *atfs-1(et15)* and *zip-3(gk3164)* animals, which have constitutively active UPR^{mt}, and WT larvae on CF18 after 48 h of feeding.

In (C)–(E) and (I), data are represented as the mean ± SD. ****$p_{adj} < 0.0001$, ***$p_{adj} < 0.001$, **$p_{adj} < 0.01$, *$p_{adj} < 0.05$; ns, not significant; one-way ANOVA with Bonferroni correction. Scale bars, 25 μm in (F) and (G) and 100 μm in (J)–(L).

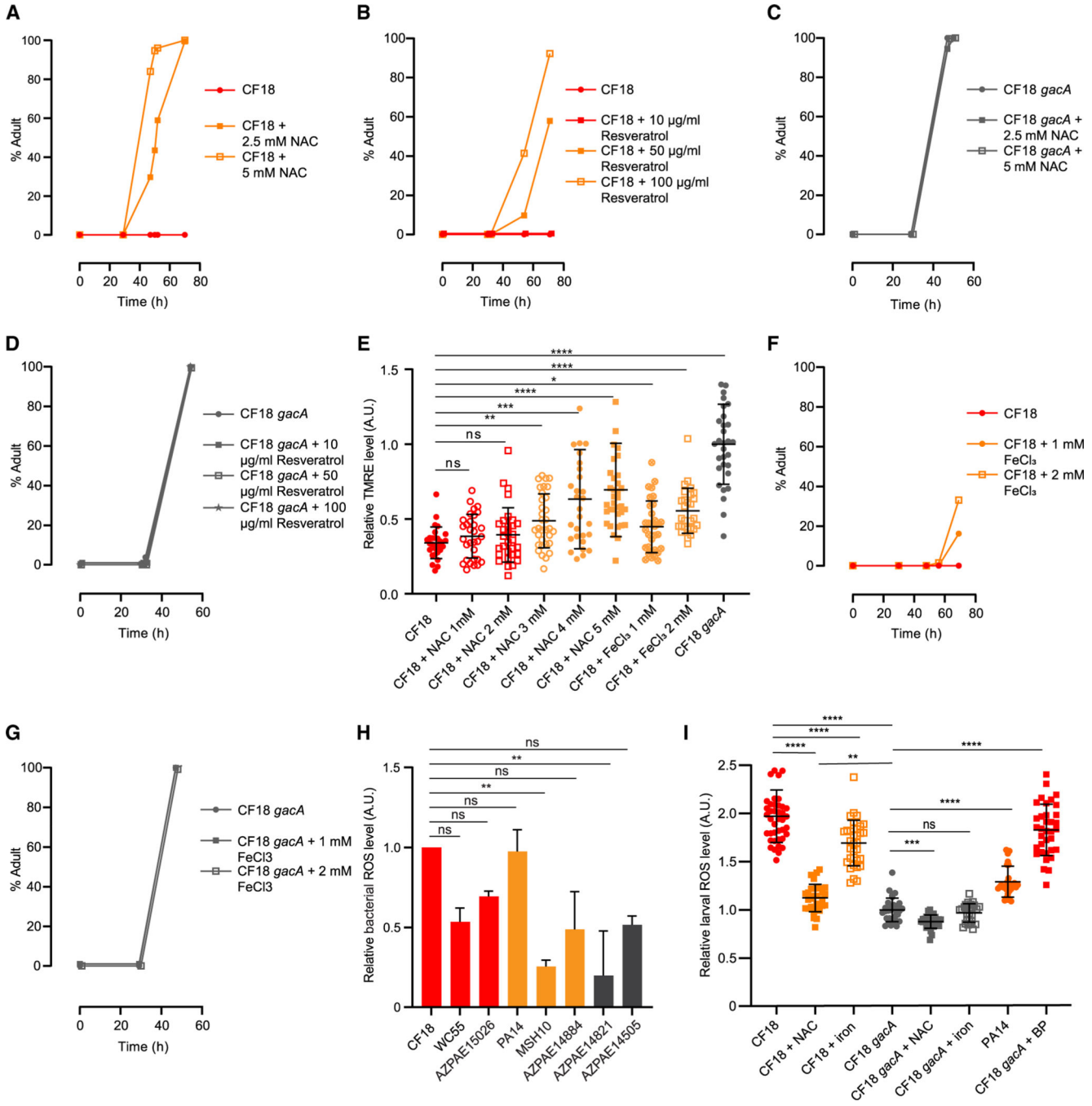

Figure 3. Supplementation of either antioxidant or iron rescue developmental and mitochondrial phenotypes

(A) Antioxidant N-acetyl-cysteine (NAC) supplementation rescued the developmental slowing of CF18-fed larvae in a dose-dependent manner. Synchronized L1 animals carrying the transgene *col-19::GFP* were seeded on slow-killing (SK) plates containing 2.5 or 5 mM NAC, and the control plates were prepared in the same manner without NAC.

(B) The antioxidant resveratrol alleviated developmental slowing of CF18-fed larvae. SK plates were supplemented with 10, 50, and 100 µg/mL resveratrol, and the assay was performed as described above.

(C) NAC supplementation did not affect the developmental rates of larvae fed CF18 *gacA* mutant.
(D) Resveratrol supplementation did not affect the developmental rates of larvae fed CF18 *gacA* mutant.
(E) NAC supplementation rescues the ΔΨm of CF18-fed larvae in a dose-dependent manner. Synchronized L1 larvae (N2) were exposed to CF18 with 0–5 mM NAC for 24 h. Error bars indicate ±SD. For each condition, 27–35 animals were quantified.
(F) Ferric chloride ($FeCl_3$) supplementation partially alleviated the developmental slowing of CF18-fed larvae.
(G) $FeCl_3$ supplementation did not affect the developmental rates of larvae fed CF18 *gacA* mutant.
(H) Bacterial ROS levels did not correlate with larval developmental rates. The mean and SD of two biological replicates are shown.
(I) NAC and iron supplementation reduced ROS levels of larvae fed CF18. Error bars indicate ±SD.
For each condition, 26–42 animals were quantified. Normal, moderately slow, and slow colored as gray, orange, and red, respectively. Representative developmental graphs of minimum two biological replicates are shown (B, C, F, and G). ****$p_{adj} < 0.0001$, ***$p_{adj} < 0.001$, **$p_{adj} < 0.01$, *$p_{adj} < 0.05$, ns, not significant by Welch's ANOVA with Dunnett's T3 correction in (E), (I), and (J) and by one-way ANOVA with Bonferroni correction in (H).

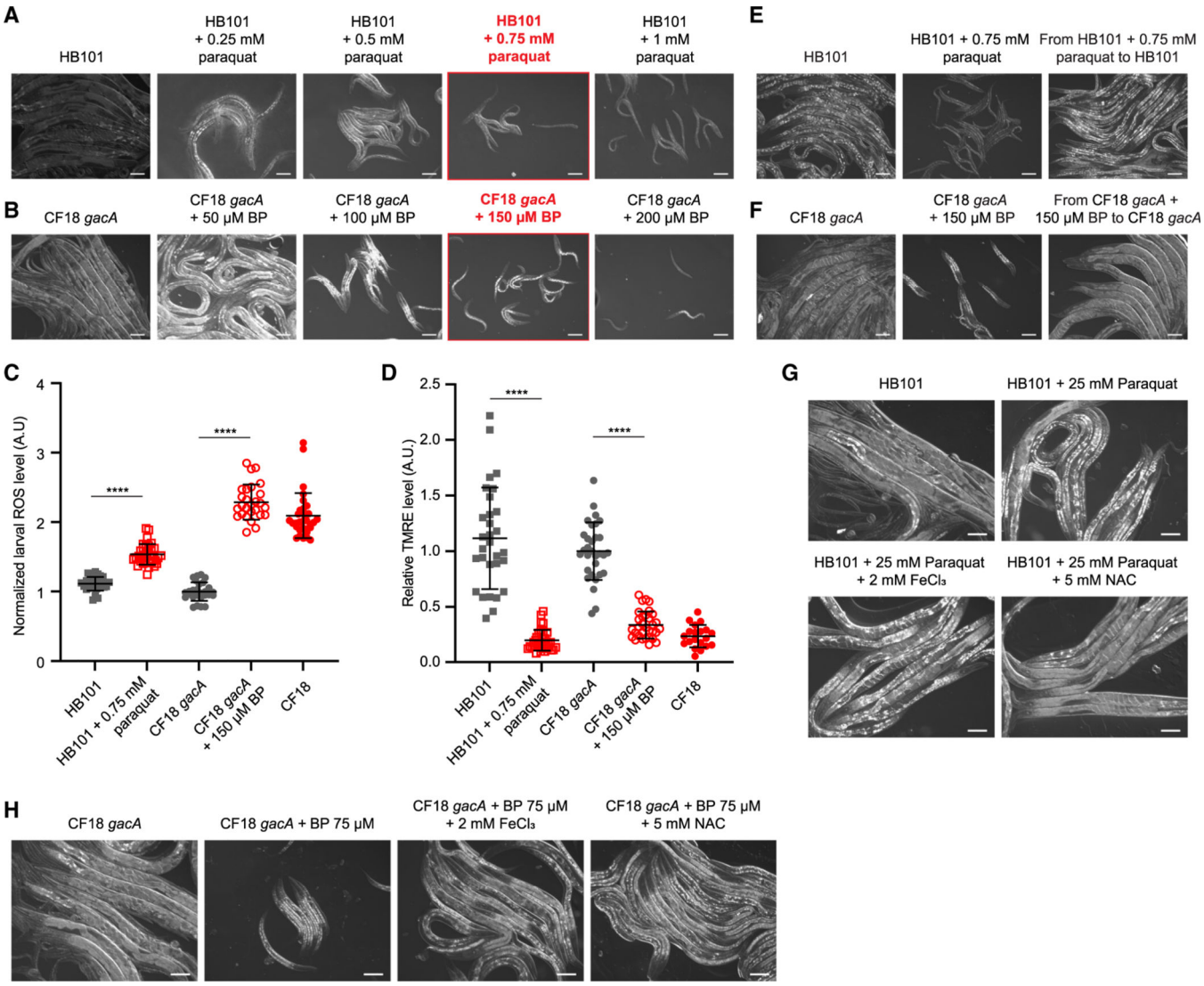

Figure 4. Induction of ROS by paraquat and chelation of iron by bipyridine (BP) phenocopied developmental and mitochondrial phenotypes of CF18

(A) Paraquat slowed larval development in a dose-dependent manner. Paraquat was added to SK plates, and then plates were seeded with the non-pathogenic *E. coli* HB101 strain. After 2 days of bacterial growth, synchronized L1 larvae were added to the plates. Imaging was performed after 2 days of incubation.

(B) BP slowed down larval development in a dose-dependent manner. BP-supplemented plates were seeded with the non-pathogenic *gacA* strain. After 2 days of bacterial growth, L1 larvae were added to the plates. Imaging was performed after 2 days of feeding.

(C) BP or paraquat supplementation of non-pathogenic *gacA* and HB101 cultures caused ROS in larvae. Error bars indicate ±SD. For each condition, 28–42 animals were quantified. ****$p_{adj} < 0.0001$ (Welch's ANOVA with Dunnett's T3 correction).

|(D) TMRE staining demonstrated that BP and paraquat disrupted ΔΨm. Error bars indicate ±SD. 20–35 animals were quantified per condition. ****$p_{adj} < 0.0001$ (Welch's ANOVA with Dunnett's T3 correction).

(E) Developmental slowing induced by paraquat was reversible upon transferring the larvae to a plate without chemicals. Larvae were exposed to the paraquat for 24 h and then transferred to HB101-seeded plates without paraquat. Before microscopy, larvae were allowed to grow for 2 days.
(F) Developmental slowing induced by BP was reversible upon transferring the larvae to a plate without BP. Larvae were exposed to BP for 24 h and then transferred to *gacA* seeded plates without chemicals. Before microscopy, larvae were allowed to grow for 2 days.
(G) 25 mM paraquat. Images were taken after 72 h of incubation.
(H) NAC supplementation shows partial rescue of developmental delay induced by 75 μM BP. Images were taken after 48 h of incubation. Scale bars, 100 μm (A, B, and E–H). Shown are representative images of two biological replicates.

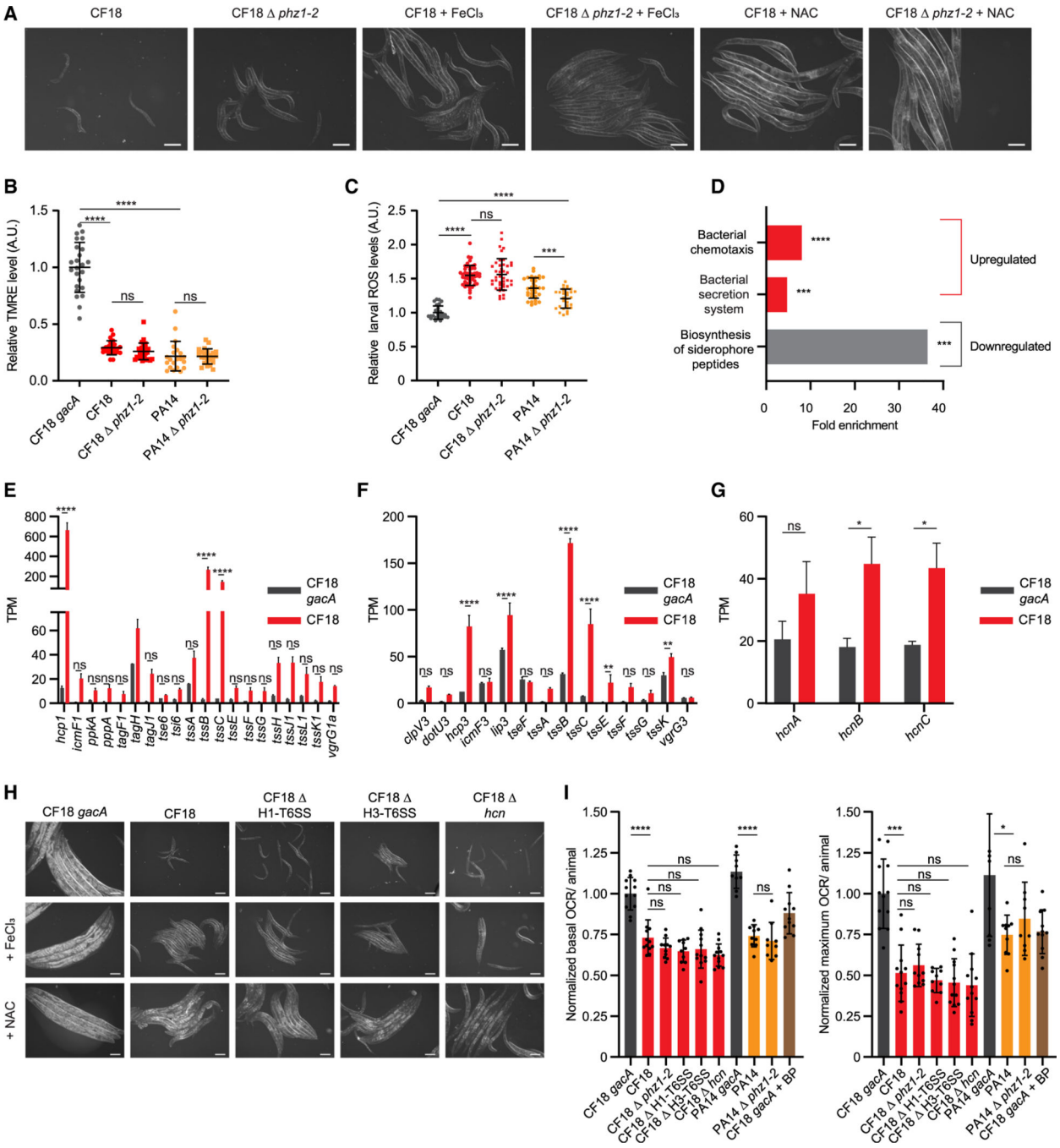

Figure 5. The genetic deletion of phenazine, H1-T6SS, H3-T6SS, or HCN operons did not alleviate developmental slowing

(A) Genetic deletion of two phenazine operons in CF18 did not alleviate development slowing. Antioxidant NAC (5 mM) and $FeCl_3$ (2mM) supplementation rescued developmental slowing of CF18 Δ *phz1–2*-fed larvae in a manner comparable with WT CF18-fed larvae. Images were taken after 72 h of feeding. Scale bars, 100 μm. Shown are representative images from two biological replicates.

(B) The deletion of phenazine operons did not improve the TMRE staining of larvae. For each condition, 21–28 animals were quantified.

(C) Quantification of MitoSOX Red fluorescence intensity of larvae fed CF18 and PA14 phenazine mutants showed that phenazine mutant-fed larvae have higher ROS levels than CF18 *gacA*-fed larvae. For each condition, 27–50 animals were quantified.
(D) Kyoto encyclopedia of genes and genomes (KEGG) pathway enrichment analysis of upregulated genes of WT CF18 (red) and downregulated genes of WT CF18 (gray) (DAVID, Benjamini correction, $p < 0.05$).
(E) TPM counts of H1-T6SS genes in WT CF18 and CF18 *gacA* mutant.
(F) TPM counts of H3-T6SS genes in WT CF18 and CF18 *gacA* mutant.
(G) TPM counts of HCN biosynthesis genes in WT CF18 and CF18 *gacA* mutant.
(H) Developmental phenotypes of larvae fed WT CF18, CF18 Δ H1-T6SS, CF18 Δ H3-T6SS, CF18 *Δ hcnA-B-C*, and CF18 *gacA* mutant at 48 h. Scale bars, 100 μm. Shown are representative images from two biological replicates.
(I) Basal and maximal OCR of animals after 4 h of feeding with the indicated bacteria. Twelve biological replicates. Data are shown as means ± SD. ****$p_{adj} < 0.0001$, ***$p_{adj} < 0.001$, **$p_{adj} < 0.01$, *$p_{adj} < 0.05$; ns, not significant by one-way ANOVA with Bonferroni correction (E−G and I) and Welch's ANOVA with Dunnett's T3 correction (B and C). In (D)−(G), two and three biological replicates of WT CF18 and CF18 *gacA*, respectively.

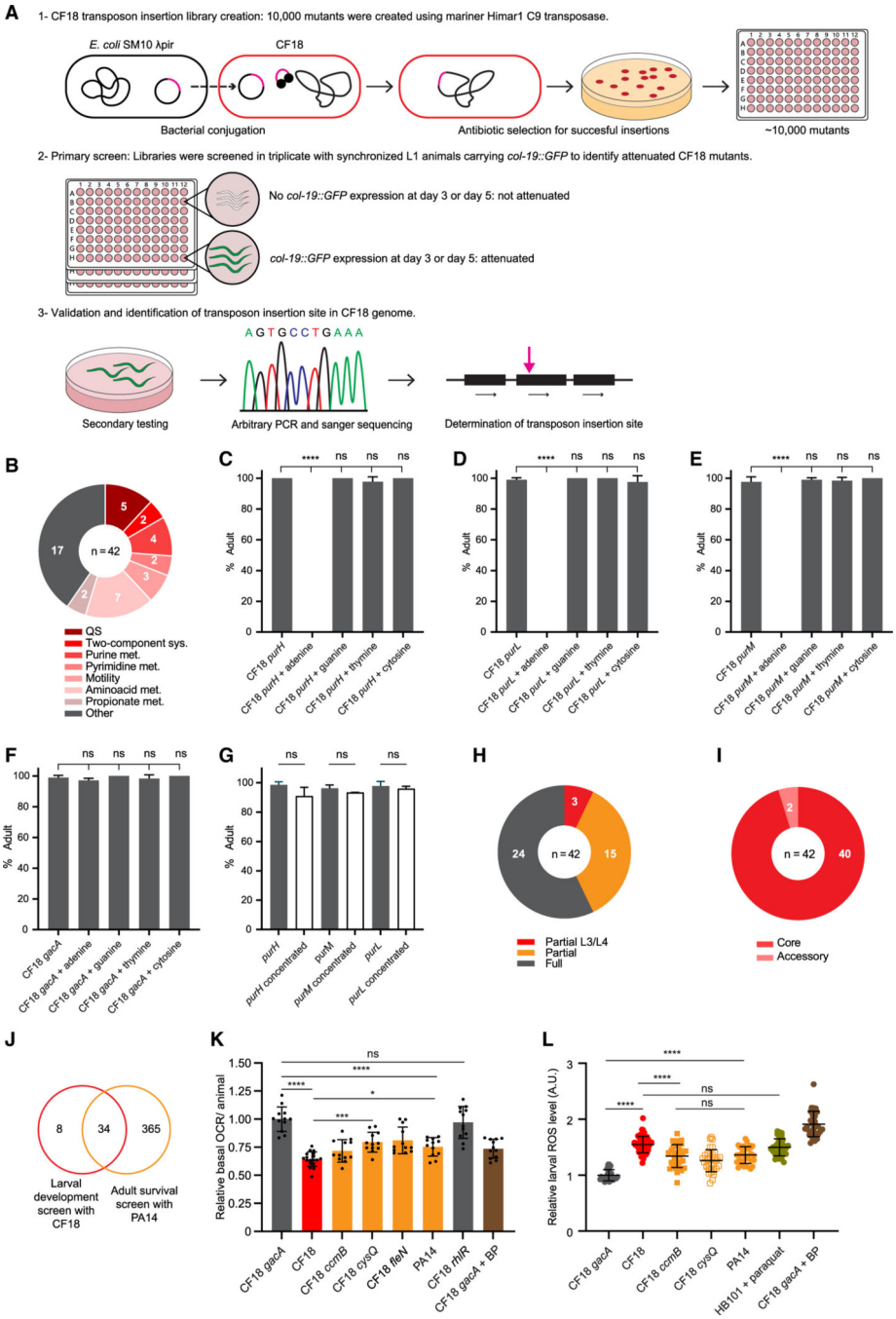

Figure 6. Transposon mutagenesis screen to identify CF18 genes that are required for developmental slowing

(A) Schematic of construction and screening of CF18 transposon insertion library of ~10,000 mutants.

(B) The functional annotation of 42 transposon mutagenesis hits. The number of hits in each category is shown.

(C) Adenine supplementation (1 mM) restored the pathogenicity of *purH*.

(D) Adenine supplementation (1 mM) restored the pathogenicity of *purL*.

(E) Adenine supplementation (1 mM) restored the pathogenicity of *purM*.

(F) Nucleotide supplementations have no effect on the CF18 *gacA* mutant.
(G) Increasing bacterial lawn density did not reverse the pathogenicity of CF18 purine mutants. Purine mutants were grown in 2.5 mL of (Luria-Bertani) LB medium and washed and concentrated prior to 48-h incubation to obtain a thick bacterial lawn.
(H) The degree to which slow growth was attenuated for CF18 mutants. Red indicates a minimal (but evident) bacterial attenuation where larvae reach the L3/L4 stage.
(I) Distribution of hits in *P. aeruginosa* genes of the core and accessory genome.
(J) Overlap between CF18 transposon mutagenesis screen with L1s and the screen by Feinbaum et al.[68] with PA14 using L4 animals. Homolog genes and the genes in the same operon/pathway are included in the overlap.
(K) Basal OCR values of larvae fed select hits after 4 h of exposure. Data were normalized to the mean OCR value of CF18 *gacA*-fed larvae. The mean and SD of 12 biological replicates are shown.
(L) Relative ROS levels of larvae fed various hits align with developmental rate. This experiment shared the same controls as in Figure 5C. Error bars indicate ±SD. For each condition, 27–50 animals were quantified.
In (H), (K), and (L), color indicates developmental rate: gray, normal; orange, moderately slow; red, slow development. In (C)–(G), (K), and (L), ****$p_{adj} < 0.0001$, ***$p_{adj} < 0.001$, **$p_{adj} < 0.01$, *$p_{adj} < 0.05$; ns: not significant by one-way ANOVA with Bonferroni correction. The mean and SD of two biological replicates are shown in (C)–(G).

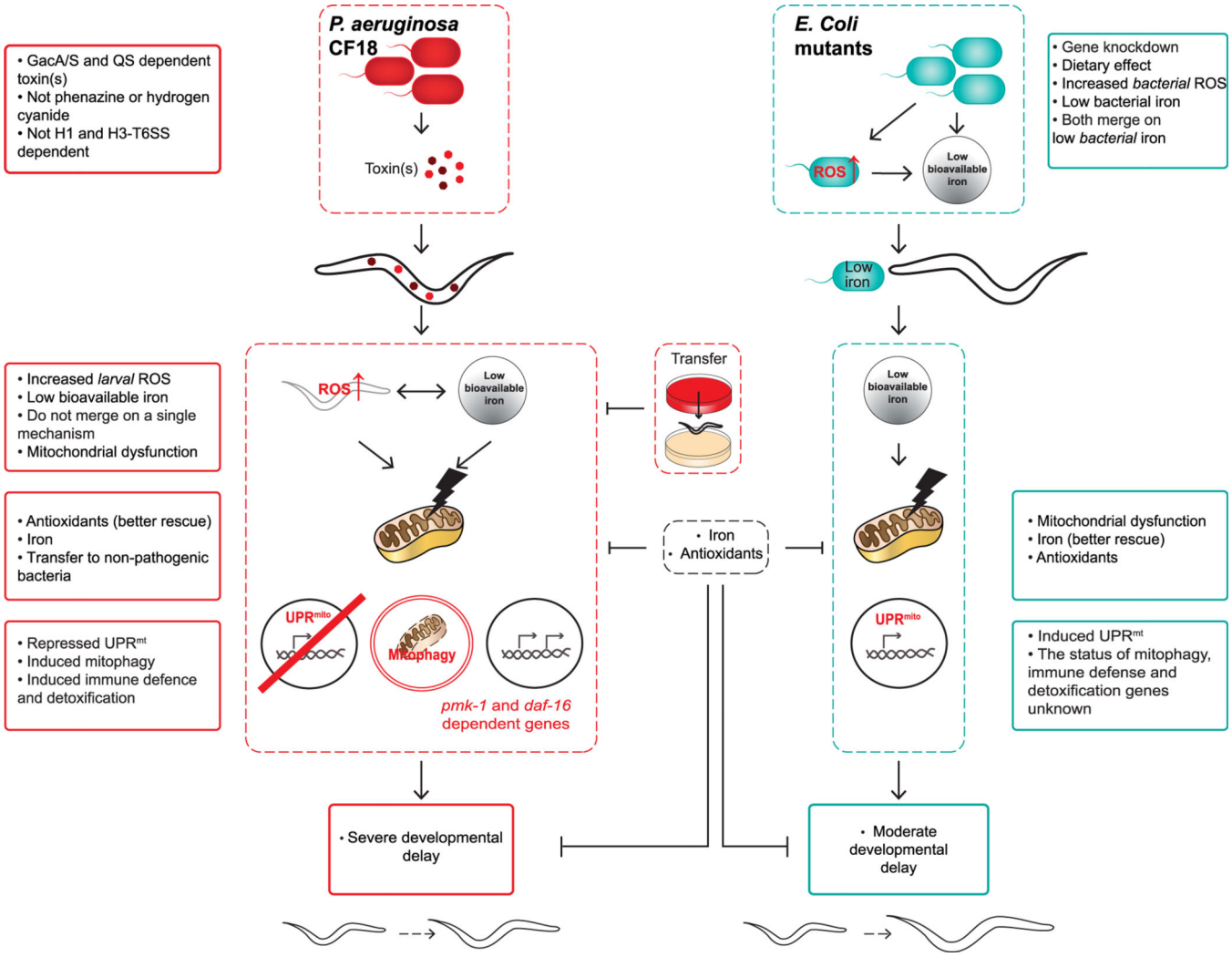

Figure 7. Model of CF18-induced developmental slowing

CF18 produces toxin(s) that are under the control of the Las, Rhl, and Pqs QS systems and GacA/S two-component system. The developmental slowing phenotype is not dependent on the known mitochondrial toxins phenazines and HCN nor on the highly upregulated H1 and H3 T6SS. These still unknown growth-slowing toxin(s) create mitochondrial dysfunction, iron imbalance, and high ROS levels in the larvae. Although the UPR^{mt} is repressed, mitophagy and immune response genes are upregulated. Developmental slowing, high ROS levels, and $\Delta\Psi m$ can be rescued by the addition of antioxidants or iron or removal of larvae from the CF18 lawns. This model for slowing of *C. elegans* development by *P. aeruginosa* CF18 is contrasted with the developmental slowing phenomenon reported for *E. coli* mutants with low bioavailable iron.[17]

KEY RESOURCES TABLE

REAGENT or RESOURCE	SOURCE	IDENTIFIER
Bacterial and virus strains		
Escherichia coli HB101	CGC	HB101
Pseudomonas aeruginosa strains	Ambros Laboratory	Table S5
P. aeruginosa CF18 transposon insertion library	This paper	N/A
Chemicals, peptides, and recombinant proteins		
N-Acetyl-L-cysteine	Sigma Aldrich	Cat#: A7250
2,2′-bipyridil	Sigma Aldrich	Cat#: D216305
Levamisole Hydrochloride	Sigma Aldrich	Cat#: PHR1798
6-carboxy-2′,7′-dichlorodihydrofluorescein diacetate	Thermo Fisher Scientific	Cat#: C400
MitoSOX™ Red	Thermo Fisher Scientific	Cat#: M36008
Tetramethylrhodamine, ethyl ester (TMRE)	Thermo Fisher Scientific	Cat#: T669
N-Acetyl-L-cysteine	Sigma Aldrich	Cat#: A7250
2,2′-bipyridil	Sigma Aldrich	Cat#: D216305
Iron(III) chloride hexahydrate	Sigma Aldrich	Cat#: 236489–100G
Deposited data		
RNA-seq data of *C. elegans* L1 larvae fed with CF18 and CF18 gacA mutant	https://www.ncbi.nlm.nih.gov/geo/	GSE213019
RNA-seq data CF18 and CF18 gacA mutant	https://www.ncbi.nlm.nih.gov/geo/	GSE213057
Experimental models: Organisms/strains		
Caenorhabditis elegans N2 (WT)	CGC	N/A
C. elegans zIcs13[*Phsp-6::GFP*]	CGC	Strain SJ4100
C. elegans ayIs6 [*[hlh-8::GFP fusion + dpy-20(+)*]	CGC	Strain PD4666
C. elegans zcIs9 [*hsp-60::GFP + lin-15(+)]*	CGC	Strain SJ4058
C. elegans maIs105 [col-19::GFP] V.	Ambros Laboratory	Strain VT1367
C. elegans muIs84 [(pAD76) sod-3p:: GFP + rol-6(su1006)]	CGC	Strain CF1553
C. elegans atfs-1(et15) V	CGC	Strain QC115

REAGENT or RESOURCE	SOURCE	IDENTIFIER
C. elegans zip-3(gk3164)	Gift from Cole Haynes, Deng et al.[72]	N/A
C. elegans pink-1(ok3538) II.	CGC	Strain RB2547
C. elegans dct-1(luc194) X.	CGC	Strain MLC2543
C. elegans pdr-1(gk448) III.	CGC	Strain VC1024
C. elegans zcIs17 [ges-1::GFP(mit)]	CGC	Strain SJ4143
C. elegans foxSi37[ges-1p::tomm-20::mKate2:: HA::tbb-2 3′ UTR] I.	CGC	Strain SJZ204
Oligonucleotides		
Primers for genotyping bacterial transposon insertion strains	https://www.idtdna.com/pages/products/custom-dna-rna/dna-oligos	Table S6
Software and algorithms		
Prism Versions 9 and 10	Graphpad	https://www.graphpad.com/scientific-software/prism/
Fiji	Schindelin et al.[73]	https://imagej.net/software/fiji/
Zen Blue	Zeiss	https://www.zeiss.com/microscopy/us/products/microscope-software.html
LAS X Core Offline Version	Leica	https://www.leica-microsystems.com/products/microscope-software/p/leica-las-x-ls/downloads/